Codimension-two bifurcations in animal aggregation models with symmetry

Buono, Pietro-Luciano; Eftimie, Raluca

Published in:
Siam Journal on Applied Dynamical Systems

DOI:
10.1137/130932272

Publication date:
2014

Document Version
Peer reviewed version

Codimension-two bifurcations in animal aggregation models with symmetry

Pietro-Luciano Buono
Faculty of Science, University of Ontario Institute of Technology
2000 Simcoe St. North
Oshawa, ONT L1H 7K4
Canada

and

Raluca Eftimie
Division of Mathematics, University of Dundee
Dundee, DD1 4HN, United Kingdom

July 8, 2014

Abstract

Pattern formation in self-organised biological aggregation is a phenomenon that has been studied intensively over the past twenty years. In general, the studies on pattern formation focus mainly on identifying the biological mechanisms that generate these patterns. However, identifying the mathematical mechanisms behind these patterns is equally important, since it can offer information on the biological parameters that could contribute to the persistence of some patterns and the disappearance of other patterns. Also, it can offer information on the mechanisms that trigger transitions between different patterns (associated with different group behaviours). In this article, we focus on a class of nonlocal hyperbolic models for self-organised aggregations, and show that these models are $\mathbf{O}(\mathbf{2})$-equivariant. We then use group-theoretic methods, linear analysis, weakly nonlinear analysis and numerical simulations to investigate the large variety of patterns that arise through $\mathbf{O}(\mathbf{2})$-symmetric codimension-two bifurcations (i.e., Hopf/Hopf, Steady-state/Hopf and Steady-state/Steady-state mode interactions). We classify the bifurcating solutions according to their isotropy types (subgroups) and we determine the criticality and stability of primary branches of solutions. We show numerically the existence of these solutions and determine scenarios of secondary bifurcations. Also, we discuss the secondary bifurcating solutions from the biological perspective of transitions between different group behaviours.

1 Introduction

Collective dynamics of self-organised aggregations is an area that has been investigated intensively over the past twenty years. The great interest in these aggregations is generated by the multitude of complex spatial and spatiotemporal patterns exhibited by them: from travelling or rotating schools of fish [43, 42], to rippling waves of Myxobacteria [29], zigzagging flocks of birds [41, 40] or various stationary aggregations. To investigate the biological mechanisms necessary for the formation and persistence of these patterns, a wide range of mathematical models (both individual-based models and continuum models – parabolic, hyperbolic and kinetic) have been proposed. These mathematical models are used to suggest plausible biological mechanisms regarding the interactions at the micro-scale level (e.g., changes in individuals' speed or turning, or changes of inter-individual social interaction ranges) that could explain the observed macro-scale level dynamics (e.g., the shape, size and dynamics of the group)[10, 21, 20, 24, 29, 23, 28, 4, 47, 2, 8, 34, 38, 39]. Generally, these models either (i) focus on numerical simulations with the purpose of comparing the simulated aggregation patterns with the available data (and thus ascertain the correctness of the micro-scale level assumptions incorporated into the models), or (ii) focus on the analytical results, e.g., show the existence of particular solutions exhibited by these models, or try to connect biological interactions at the micro-scale and macro-scale levels [12]. The first approach can be found mainly in individual-based models, for which studies into the mathematical mechanisms behind the patterns are still a difficult task. The second approach can be found in continuum models, for which numerical simulations can sometimes become too complicated (see the review in [12]). There are, however, models that combine analytical results with numerical simulations. For example Fetecau and Eftimie[16] showed that discontinuous kernels could cause gradient blow-up patterns. Focusing on milling patterns (i.e., rotating groups of individuals), Chuang et al. [9] have shown that the hydrodynamics framework can support these patterns, but it cannot support the double milling patterns (groups formed if individuals rotate in both directions), due to velocity averaging inside a mesh cell.

In general, these models for self-organised aggregations (either individual-based or continuum models) exhibit only a few types of patterns: stationary pulses (resting aggregations)[45], travelling pulses (migrating aggregations)[36] or tori (rotating aggregations)[44]. Moreover, these models usually associate specific patterns to specific parameter values, with eventual transitions between patterns being correlated to changes in parameter values [10]. One type of models that has been shown to exhibit a much larger variety of patterns was introduced in [14, 13]. There, the authors developed a class of nonlocal hyperbolic models for self-organised aggregations, which incorporate different ways individuals could interact with their neighbours based on different communication mechanisms. Numerical investigations of these models have shown that they can exhibit various spatial and spatio-temporal patterns: from classical stationary and travelling waves, to travelling trains and quasi periodic solutions, and even more exotic patterns (such as ripples and feather-like patterns) [13]. The bifurcation of some of the simpler patterns, namely travelling trains and stationary pulses, has been investigated in [15] for one particular communication sub-model (called M2) via weakly nonlinear analysis. In particular, it was shown

that these two patterns arise through subcritical Hopf and Steady-state (codimension-1) bifurcations, suggesting that the persistence of these patterns requires a density threshold mechanisms (i.e., groups that have a population density higher than a certain threshold – which depends on some bifurcation parameter – will persist for very long term, while groups that have a population density lower than this threshold will disperse). This mechanism has actually been observed in nature (e.g., in ants [3] and locusts [6]).

The goal of this article is to focus on the class of nonlocal hyperbolic models introduced in [14, 13], and to investigate the role of model symmetries on the formation of various patterns. Mathematically, the occurrence of symmetry in differential equations leads to many interesting consequences, such as multiple bifurcating branches at a bifurcating point and enable a classification of solutions using their symmetry group. Biologically, understanding and classifying the bifurcation dynamics of the observed patterns allows us to understand the transitions between different patterns (i.e., between different group behaviours). In particular, if multiple bifurcating branches (which are usually associated with different behaviours/patterns) exist for similar parameter values, it could suggest that transitions between patterns might not always be associated with changes in parameter values (i.e., such transitions could be intrinsic to the models, being associated with secondary or tertiary bifurcations from unstable patterns [7]). Also, understanding the bifurcation dynamics of the model allows us to understand how asymmetries in the interactions between individuals (e.g., asymmetric communication) could influence the patterns observed at the group level. This aspect is related to the symmetry-breaking process, and it is known to correlate to increased complexity in biological systems [32].

The main contributions of this paper are the following. We begin by showing that all communication-based sub-models from [13] defined on a finite domain [0,L] with periodic boundary conditions are invariant with respect to the symmetry group $\mathbf{O}(\mathbf{2})$. Using this symmetry perspective, we then discuss steady-state solutions and their symmetry properties. We focus on the $\mathbf{O}(\mathbf{2})$-symmetric steady-states and investigate the linearization using group-theoretic methods as outlined in [19, 18]. In particular, symmetry enables one to decompose the tangent space at steady-state solutions into symmetry-invariant subspaces (i.e., the isotypic decomposition). The existence of so many patterns in the nonlocal hyperbolic models introduced in [13], raises the question of possible codimension-two bifurcations. Therefore, we consider one particular sub-model (model M4 in [13]) and show that it can display Steady-state/Steady-state (SS/SS), Steady-state/Hopf (SS/H) and Hopf/Hopf (H/H) codimension-two bifurcations with $\mathbf{O}(\mathbf{2})$ symmetry. In a recent paper [7], we partially investigated the patterns emerging near the H/H bifurcation via weakly-nonlinear analysis [7]. In this paper, we focus mainly on the SS/H and SS/SS codimension-two bifurcations for which we classify the eigenfunction patterns that arise near these codimension-two bifurcations. The contour plots of the eigenfunctions associated with various isotropy types (subgroups) at bifurcation gives an approximation of the main patterns emerging from the SS/H bifurcation point. This is particularly useful as a tool to distinguish between patterns obtained by numerically solving the full model. For a different class of models (describing Taylor-Couette flows) Hill and Stewart [25] studied the $\mathbf{O}(\mathbf{2})$-symmetric SS/H mode interactions: they determined the normal form equations (after centre manifold or Lyapunov-Schmidt reduction), obtained branching equations and then computed the eigen-

values of the bifurcating branches (to investigate the stability of these branches). Here, we follow their approach to investigate the neighborhood of the SS/H point. In particular, we show that the amplitude equations to third order derived via a rigorous weakly nonlinear analysis are $\mathbf{O}(\mathbf{2})$-equivariant and identical to the third order truncation of the normal form equations from [25]. We determine primary bifurcating branches (stationary pulse, rotating waves and standing waves) and their stability and discuss scenarios for secondary bifurcations. Finally, we discuss the stability of bifurcating branches and the existence of secondary bifurcations from a biological perspective.

In Section 2 we present the model and the symmetry properties. This section also contains a discussion of the steady-states. In Section 3 we show a detailed analysis of the linearization near the $\mathbf{O}(\mathbf{2})$-symmetric steady-state using group-theoretic methods. Codimension-two bifurcation points are discussed in Section 4. In this section we also describe the linear eigenfunctions at bifurcations, plot them and compare with numerical simulations. Section 5 presents the bifurcation results from the weakly-nonlinear analysis and we discuss secondary bifurcation scenarios. The paper concludes with a discussion section, which includes also a description of future research problems.

2 The model

The following 1D model of hyperbolic partial differential equations describes the evolution of densities of right-moving (u^+) and left-moving (u^-) individuals, which travel with constant velocity γ and change their movement direction from right to left (with rate λ^+) and from left to right (with rate λ^-) [13]:

$$\partial_t u^+(x,t) + \partial_x(\gamma u^+(x,t)) = -\lambda^+[u^+,u^-]u^+(x,t) + \lambda^-[u^+,u^-]u^-(x,t), \tag{1a}$$

$$\partial_t u^-(x,t) - \partial_x(\gamma u^-(x,t)) = \lambda^+[u^+,u^-]u^+(x,t) - \lambda^-[u^+,u^-]u^-(x,t), \tag{1b}$$

$$u^\pm(x,0) = u_0^\pm(x). \tag{1c}$$

The density-dependent turning rates $\lambda^\pm$ describe the social response of an individual to the signals received from its neighbours. This social response can be: attraction towards individuals further away ($y_a^\pm$), repulsion from nearby neighbours ($y_r^\pm$) or alignment with neighbours at intermediate distances ($y_{al}^\pm$):

$$\lambda^\pm[u^+,u^-] = \lambda_1 + \lambda_2 f(y_r^\pm[u^+,u^-] - y_a^\pm[u^+,u^-] + y_{al}^\pm[u^+,u^-]), \tag{2}$$

$$= \Big(\lambda_1 + \lambda_2 f(0)\Big) + \lambda_2\Big(f(y_r^\pm - y_a^\pm + y_{al}^\pm) - f(0)\Big). \tag{3}$$

The terms $\lambda_1 + \lambda_2 f(0)$ and $\lambda_2\big(f(y^\pm) - f(0)\big)$ describe the baseline random turning rate and the bias turning rate, respectively. These assumptions of a random and a bias turning rates are biologically realistic, since, as noted by Lotka [33], "the type of motion presented by living organisms ... can be regarded as containing both a systematically directed and also a random element". When $f(0) \ll 1$, we can approximate the random turning by λ_1 and the bias turning by $\lambda_2 f(y^\pm)$. For biological realism, we consider f to be a positive, increasing and bounded

function that depends on the attractive/repulsive/alignment social interactions mentioned previously. (An example of such function is $f(y) = 0.5 + 0.5\tanh(y)$ [13].) Since attraction and repulsion have opposite effects, note that they enter equation (3) with different signs. Eftimie et al. [13] pointed out that whether individuals turn away or towards their neighbours depends on whether they can perceive these neighbours. Therefore, function f should contain mechanisms through which individuals can emit/perceive signals to/from their neighbours. To address this issue, Eftimie et al. [13] defined the attractive, repulsive and alignment interactions in terms of the possible communication mechanisms among group members. This lead to the derivation of five possible models, labelled M1 to M5, each describing a particular interaction (via a communication mechanism) between individuals (see Table 1). These interactions depend on whether a reference individual perceives its neighbours (positioned ahead or behind it) moving in the same or opposite direction. A detailed description of models M1-M5 can be found in [13].

Table 1: Nonlocal social interaction terms ($y_j^{\pm}$, $j \in \{a, al, r\}$) introduced in [13]. Constants q_a, q_{al}, q_r describe the magnitudes of the attractive, alignment and repulsive interactions, respectively. Kernels $K_{a,al,r}(s)$ describe the spatial ranges for each of these social interactions. Note that $u = u^+ + u^-$.

Communication models	Interaction terms: attraction ($y_a^{\pm}$), repulsion ($y_r^{\pm}$), alignment ($y_{al}^{\pm}$)
M1	$y_{a,r}^{\pm} = q_{r,a}\int_0^{\infty} K_{a,r}(s)\big(u(x \pm s) - u(x \mp s)\big)ds$
	$y_{al}^{\pm} = q_{al}\int_0^{\infty} K_{al}(s)\big(u^{\mp}(x \pm s) - u^{\pm}(x \mp s)\big)ds$
M2	$y_{a,r}^{\pm} = q_{r,a}\int_0^{\infty} K_{a,r}(s)\big(u(x \pm s) - u(x \mp s)\big)ds$
	$y_{al}^{\pm} = q_{al}\int_0^{\infty} K_{al}(s)\big(u^{\mp}(x \mp s) + u^{\mp}(x \pm s) - u^{\pm}(x \mp s) - u^{\pm}(x \pm s)\big)ds$
M3	$y_{r,a}^{\pm} = q_{r,a}\int_0^{\infty} K_{r,a}(s)u(x \pm s)ds$
	$y_{al}^{\pm} = q_{al}\int_0^{\infty} K_{al}(s)\left(u^{\mp}(x \pm s) - u^{\pm}(x \pm s)\right)ds$
M4	$y_{r,a}^{\pm} = q_{r,a}\int_0^{\infty} K_{r,a}(s)\left(u^{\mp}(x \pm s) - u^{\pm}(x \mp s)\right)ds$
	$y_{al}^{\pm} = q_{al}\int_0^{\infty} K_{al}(s)\left(u^{\mp}(x \pm s) - u^{\pm}(x \mp s)\right)ds$
M5	$y_{a,r}^{\pm} = q_{r,a}\int_0^{\infty} K_{a,r}(s)u^{\mp}(x \pm s)ds$
	$y_{al}^{\pm} = q_{al}\int_0^{\infty} K_{al}(s)u^{\mp}(x \pm s)ds$

Parameters q_j, $j = r, a, al$, that appear in front of the integrals in Table 1, describe the magnitude of the repulsive (r), attractive (a) and alignment (al) interactions. Kernels $K_{r,a,al}$ indicate whether the interactions take place inside the repulsion range (K_r), attraction range (K_a) or alignment range (K_{al}). Although these kernels can be described by a variety of continuous and discontinuous functions [12], in this article we consider only translated Gaussian kernels:

$$K_j(s) = \frac{1}{2\pi m_j^2} e^{-(s-s_j)^2/(2m_j^2)}, \text{ with } j = r, a, al, \text{ and } m_j = s_j/8. \tag{4}$$

Here, s_j, $j = r, a, al$ describe the length of interaction ranges. The description of model (1) is completed by imposing periodic boundary conditions on a finite domain of length L: $u^{\pm}(0,t) = u^{\pm}(L,t)$. These conditions approximate the motion of organisms on an infinite domain. Note that this type of boundary conditions has an impact on the symmetries of the system, as we show below. A more detailed description of model (1) with all its sub-models can be found in [13].

For the bifurcation analysis in this paper, we focus on one particular mechanism (model M4 in [13] and Table 1), where the turning behaviour of an individual is influenced only by the information it receives from neighbours facing towards it (see Figure 1). More precisely, we assume that a reference individual at position x changes its moving direction only upon interaction with neighbours at $x+s$ moving left towards it (i.e, $u^-(x+s)$ neighbours) and with neighbours at $x-s$ moving right towards it (i.e., $u^+(x-s)$ neighbours). We assume here that individuals moving away from the reference individual cannot be perceived. This assumption can describe, for example, communication through directional sound signals, as observed in some species of birds [5, 48]. To decide its movement direction, the individual at x weighs the information received from all neighbours ahead and behind it within an interaction range, i.e., $\int_0^\infty K_j(s)(u^{\mp}(x \pm s) - u^{\pm}(x \mp s))ds$ (see also Table 1). If this integral is positive, the interaction term $y_j^{\pm}$ is positive, and thus the turning rate increases. Otherwise, the turning rate is close to zero, and the individual keeps moving in the same direction.

To simplify our analysis, throughout most of this paper we ignore the alignment interactions (i.e., $q_{al} = 0$). We only look at the case with $q_{al} > 0$ when investigating the Steady-state/Steady-state mode interactions in Section 4. This assumption of zero alignment reduces the applicability of model (1) to biological aggregations where organisms interact only via attractive and repulsive interactions (e.g., swarms of insects).

2.1 O(2)-symmetry of the models

In this section, we show that all five models M1-M5 in Table 1 are $\mathbf{O(2)}$-invariant. Let $T_z : \mathbb{R} \to \mathbb{R}$ be the translation operator by $z \in \mathbb{R}$: $T_z(x) = x + z$. Then the group of all translations T_z is isomorphic to $\mathbb{R}$. This operator acts on functions u via the domain of u:

$$(T_z.u)(x) := u(T_{-z}(x)) = u(x - z). \tag{5}$$

We begin the discussion of the symmetries of model (1) by noting that $\lambda^{\pm}$ are T_z-invariant because the integrals in Table 1 are translation invariant. Rewriting system (1) as

$$\begin{aligned}
\partial_t u^+(x,t) &= -\lambda^+ u^+(x,t) + \lambda^- u^-(x,t) - \partial_x(\gamma u^+(x,t)) = F_1(u^+, u^-),\\
\partial_t u^-(x,t) &= \lambda^+ u^+(x,t) - \lambda^- u^-(x,t) + \partial_x(\gamma u^-(x,t)) = F_2(u^+, u^-),
\end{aligned}$$

and considering the T_z-invariance of $\lambda^{\pm}$ and the translation invariance of ∂_x, we obtain

$$F_i(T_z.(u^+, u^-), t) = T_z.F_i(u^+, u^-, t), \quad i = 1, 2.$$

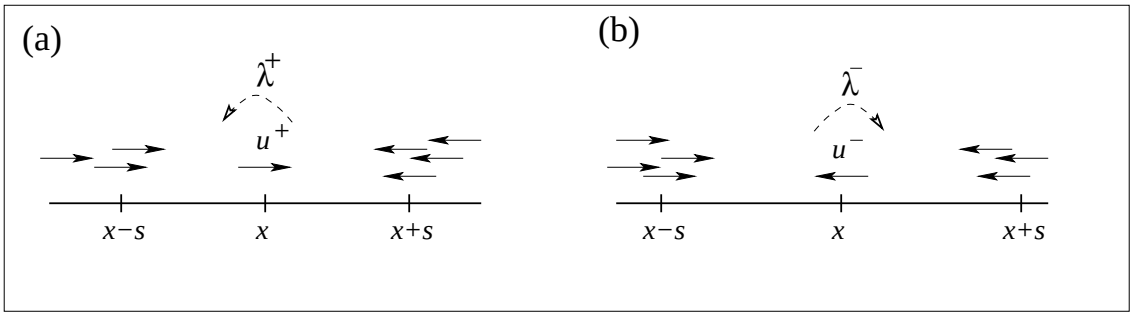

Figure 1: The behaviour of a reference individual positioned at x upon interaction with its neighbours positioned at $x+s$ and $x-s$. Here s can be inside the repulsion/alignment/attraction ranges – depending on the interaction kernel $K_j(s)$, $j = r, al, a$, used to describe the nonlocal interactions (see also Table 1). (a) A right-moving individual (u^+); (b) A left-moving individual (u^-). The reference individual at x will change its direction of movement (with rate $\lambda^{\pm}$) only after receiving information from those neighbours moving towards it.

Hence, equation (1) is T_z-equivariant. Because of the periodic boundary conditions imposed on (1) on the interval $[0, L]$, the action of the translation group on solutions (u^+, u^-) of (1) is isomorphic to $\mathbb{R}/L\mathbb{Z} \simeq \mathbf{SO}(\mathbf{2})$ and we use $\theta \in [0, L]$ to parametrize $\mathbf{SO}(\mathbf{2})$. We now introduce the following $\mathbb{Z}_2$ action on pairs of functions (u^+, u^-):

$$\kappa.(u^+(x), u^-(x)) = (u^-(L-x), u^+(L-x)). \tag{6}$$

Concretely, the κ action sends right moving individuals at x to left moving individuals at $L-x$ and vice-versa. Naturally, the turning rate attached to u^+ at x becomes the turning rate of u^- at $L-x$ via κ, that is: $\kappa.\lambda^+(x) = \lambda^-(L-x)$. This can be verified algebraically by looking at the expressions for the repulsion, attraction and alignment formulae. Consider for instance the M4 model (see Table 1). The terms describing the social interactions for a right-moving individual (+) are transformed as follows under the action of κ:

$$\begin{aligned} \kappa.y_j^+(x) &= q_j \int_0^\infty K_j(s)(u^+(L-(x+s)) - u^-(L-(x-s)))\, ds \\ &= q_j \int_0^\infty K_j(s)(u^+(L-x-s)) - u^-(L-x+s)))\, ds = y_j^-(L-x), \end{aligned} \tag{7}$$

for $j = r, a, al$. We remark here that all other communication models shown in Table 1 have the same property because in all cases, as u^+ is changed for u^-, $x+s$ goes to $x-s$ and vice-versa.

Finally, it is easy to check that $T_\theta \circ \kappa = \kappa \circ T_{-\theta}$. Thus, $\mathbf{O}(\mathbf{2}) \simeq \mathbf{SO}(\mathbf{2}) \rtimes \mathbb{Z}_2(\kappa)$ acts on $(u^+(x), u^-(x))$. The $\mathbf{O}(\mathbf{2})$-invariance of (1) is verified by showing that if $(u^+(x), u^-(x))$ is a solution, then $\kappa.(u^+(x), u^-(x))$ is also a solution. We can rewrite system (1) as

$$\pm u_t^{\pm} - \gamma u_x^{\pm} = -\lambda^+(x)u^+ + \lambda^- u^- = F_1(u^+, u^-).$$

Then, substituting $(u^+(x,t), u^-(x,t)) \to (u^-(L-x,t), u^+(L-x,t))$ we obtain

$$\begin{aligned} \pm u_t^{\mp}(L-x,t) - \gamma u_x^{\mp}(L-x,t) &= F_1(u^-(L-x,t), u^+(L-x,t)), \\ -(\pm u_t^{\pm}(L-x,t) + \gamma u_x^{\mp}(L-x,t)) &= -F_1(u^+(L-x,t), u^-(L-x,t)), \end{aligned}$$

where, since $\kappa.\lambda^+(x) = \lambda^-(L-x)$, we have

$$F_1(u^-(L-x,t), u^+(L-x,t)) = -F_1(u^+(L-x,t), u^-(L-x,t)).$$

This result is summarized in the following statement:

Proposition 2.1 *The five systems of partial differential equations (1) labelled M1 to M5, defined on* $[0,L]$ *with periodic boundary conditions* $u^\pm(0,t) = u^\pm(L,t)$ *are* $\mathbf{O}(\mathbf{2})$*-invariant, where* $\mathbf{O}(\mathbf{2})$ *acts on solutions of (1) via (5) and (6).*

We begin our analysis of system (1) with a brief look at the steady-state solutions.

2.2 Steady-states

The steady-states of the model are obtained by setting the time derivatives $\partial_t u^\pm = 0$ in (1). For the remainder of this section, we drop the time dependence of $u^\pm$. As shown in Eftimie [11], the steady-state solutions must satisfy

$$\begin{aligned} \gamma \partial_x u^+(x) &= -\lambda^+ u^+(x) + \lambda^- u^-(x), \\ -\gamma \partial_x u^-(x) &= \lambda^+ u^+(x) - \lambda^- u^-(x). \end{aligned}$$

Since the equations for u^+ and u^- are now equal, it implies that $\partial_x u^+(x) = \partial_x u^-(x)$. Therefore, all steady-states must satisfy

$$u^-(x) = u^+(x) + C, \tag{8}$$

where C is some arbitrary constant. Note that if $u^-(x_0) = u^+(x_0)$ for some $x_0 \in [0,L]$, then $C = 0$. The case where equation (1) is defined on $\mathbb{R}$ is briefly discussed in [11] where it is shown that if $u^+(\pm\infty) = u^-(\pm\infty) = 0$ then $C = 0$.

In our context, we impose the boundary conditions $u^\pm(0) = u^\pm(L)$ which implies the $\mathbf{O}(\mathbf{2})$ symmetry of the model. To classify the solutions with respect to their symmetry groups, we define isotropy subgroups and fixed-point subspaces as follows. Consider the action of a group Γ on a vector space V. The *isotropy subgroup* of the point $v \in V$ is

$$\Gamma_v := \{\rho \in \Gamma \mid \rho.v = v\}.$$

Let Σ_1 and Σ_2 be two subgroups. Σ_1 and Σ_2 are conjugate in Γ if there exists $\gamma \in \Gamma$ such that $\gamma^{-1}\Sigma_1\gamma = \Sigma_2$. The *conjugacy class* of Γ_v consists of all isotropy subgroups conjugate to Γ_v, and it is called the *isotropy type*. In particular, if $v_1, v_2 \in V$ are on the same *group orbit* ($v_1 = \gamma v_2$ for some $\gamma \in \Gamma$) then v_1 and v_2 have the same isotropy type. It is common [19, 18] to keep using isotropy subgroup rather than the more accurate isotropy type when discussing the classification of solutions with respect to symmetry, but one must always keep in mind that the results are valid for the whole group orbit.

For an isotropy subgroup $\Sigma \subset \Gamma$, the *fixed point subspace* of Σ is

$$\mathrm{Fix}(\Sigma) = \{v \in V \mid \sigma.v = v, \text{ for all } \sigma \in \Sigma\}.$$

We have the following result.

Theorem 2.2 *If $(u^+(x), u^-(x))$ is a steady-state solution of (1) with isotropy subgroup Σ and $(\theta, \kappa) \in \Sigma$ for some $\theta \in [0, L]$, then $u^+(x) = u^-(x)$.*

Proof: Consider a steady-state solution $(u^+(x), u^-(x))$ of (1), which satisfies equation (8). Without loss of generality we can assume that $(u^+(x), u^-(x))$ is κ-symmetric. Then,

$$\kappa.(u^+(x), u^-(x)) = (u^-(L-x), u^+(L-x)) = (u^+(x), u^-(x)).$$

This means that $u^{\mp}(L-x) = u^{\pm}(x)$. In particular set $x = L/2$, from which we have $u^-(L/2) = u^+(L/2)$. Substituting these values of $u^{\pm}(L/2)$ into equation (8) forces $C = 0$ (with C the arbitrary constant in (8)). Therefore $u^+(x) = u^-(x)$ on $[0, L]$. ∎

In general, the steady-states are solutions to the boundary value problem

$$\gamma \partial_x u(x) = \big(-\lambda^+[u] + \lambda^-[u] \big) u(x) + \lambda^-[u] C, \qquad u(0) = u(L). \tag{9}$$

Equation (9) is an advanced-retarded distributed functional differential equation, or a mixed-type distributed functional differential equation. After simplifying the terms in the parenthesis, one obtains

$$\gamma \partial_x u(x) = -0.5\lambda_2 \left(\tanh(y_r^+ - y_a^+ + y_{al}^+) - \tanh(y_r^- - y_a^- + y_{al}^-) \right) u(x) + \lambda^-[u] C.$$

with boundary conditions $u(0) = u(L)$. An interesting family of non-homogeneous steady-state solutions of (1) are the $\mathbf{D}_n$-symmetric spatially periodic patterns. These can be obtained from symmetry-breaking steady-state bifurcation from an $\mathbf{O(2)}$ symmetric equilibrium of (1) as shown below.

Another way of studying these $\mathbf{D}_n$-symmetric patterns would be via Hopf bifurcation directly from (9). Recent results about Hopf bifurcation in mixed-type functional differential equations have been obtained by Hupkes and Verduyn-Lunel [27] for fixed shift using centre manifold reduction and by Guo [22] in the fixed shift equivariant case using Lyapunov-Schmidt reduction. Note that (9) has distributed shifts and so the results in [22] would need to be generalized to this case.

We now focus on the case of homogeneous solutions, $u^+(x) = u_+^*$ and $u^-(x) = u_-^*$ where u_+^* and u_-^* are constants and $u_+^* + u_-^* = A$, where the total population density $A = \frac{1}{L}\int_0^L (u^+(x) + u^-(x))dx$ is fixed. Because the kernels are given by Gaussian functions and $u^{\mp} - u^{\pm} = \mp C$, a simple calculation shows that the terms λ^+ and λ^- have constant values. Thus, homogeneous steady-state solutions are solutions of the algebraic equation

$$0 = -\lambda^+ u_+^* + \lambda^-(A - u_+^*).$$

It is shown in [14, 13] that model (1) can have up to five spatially homogeneous steady states of the form: $(u^+, u^-) = (u^*, A - u^*)$ or $(u^+, u^-) = (A - u^*, u^*)$ (throughout this article we assume $A = 2$). The steady state $(u^+, u^-) = (A/2, A/2)$ exists for all parameter values, and is left fixed by (5) and (6). In fact, all elements of $\mathrm{Fix}(\mathbf{O(2)})$ are of the form $(A/2, A/2)$ for some $A \geq 0$. Moreover, $\kappa.(u^*, A - u^*) = (A - u^*, u^*)$ and so these equilibria are on the same group orbit. The steady-states of the form $(u^*, A - u^*)$ are fixed by any translation (5), and therefore have the isotropy subgroup $\mathbf{SO}(2)$.

Remark 2.3 The existence of the four states with $u^{\pm} \neq A/2$ depends on particular parameter values (see Figure 2 for model M4). Since these steady states are not all unstable at the same time [14], it is possible that a solution that starts near an unstable state eventually approaches a stable spatially homogeneous state. We return to this aspect in Section 4.2 in the context of numerical simulations of patterns near codimension-two points.

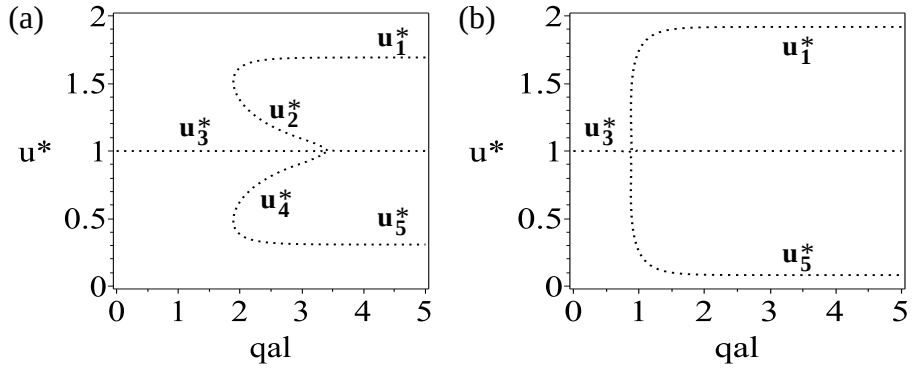

Figure 2: Spatially homogeneous steady states exhibited by equation (1) corresponding to model M4, for different values of λ_2. (a) For $\lambda_2 = 0.9$, there are five steady states. (b) For $\lambda_2 = 4.5$, there are three steady states. The other parameter values are $\lambda_1 = 0.2$, $A = 2.0$, $\gamma = 0.1$, $q_a = 2.0$, $q_r = 2.0$.

3 The Linear Operator

The focus in this paper is on the bifurcations of heterogeneous patterns from an homogeneous steady-state $(A/2, A/2)$ with isotropy subgroup $\mathbf{O}(\mathbf{2})$. The results in the previous sections are valid for all sub-models M1-M5 described in Table 1. Now, we restrict our analysis to model M4 which, as it is shown in the next sections, can display all three types of codimension-two bifurcations with $\mathbf{O}(\mathbf{2})$ symmetry (i.e., Hopf/Hopf, Steady-state/Hopf, Steady-state/Steady-state). We note that it is possible that other sub-models could also exhibit these bifurcations. However, it is not the goal of this article to investigate all codimension-two bifurcations in all sub models M1-M5. Rather, it is to show the reader that such bifurcations can exist in one single model.

3.1 Model M4: computing the linear term $\mathcal{L}$

To linearise equations (1), consider small perturbations of the spatially homogeneous steady states $u^* = A/2$: $u^{\pm} = u^* + u_1^{\pm}$, with $u_1^{\pm} \ll 1$. Substituting these values into equations (1), expanding $\lambda^{\pm}[u^* + u_1^+, u^* + u^-]$ in Taylor series (i.e., $\lambda^{\pm} \approx \lambda_1 + \lambda_2[f(0) + f'(0)(y_r^{\pm} - y_a^{\pm})] + \cdots$), neglecting the nonlinear terms and finally introducing the notations $L_1 = \lambda_1 + \lambda_2 f(0)$, $R_1 = \lambda_2 f'(0)$ and $K(s) := q_r K_r(s) - q_a K_a(s) + q_{al} K_{al}(s)$, leads to the following linearised model M4:

$$\partial_t u_1^+ + \partial_x(\gamma u_1^+) = -L_1(u_1^+ - u_1^-) - R_1 u^* \int_0^\infty K(s)(u_1^-(x+s) - u_1^+(x-s) - u_1^+(x-s) + u_1^-(x+s))\,ds, \tag{10a}$$

$$\partial_t u_1^- - \partial_x(\gamma u_1^-) = L_1(u_1^+ - u_1^-) + R_1 u^* \int_0^\infty K(s)(u_1^-(x+s) - u_1^+(x-s) - u_1^+(x-s) + u_1^-(x+s))\,ds. \tag{10b}$$

To simplify these equations, let us define $K^+ * v := \int_0^\infty K(s)v(x+s)\,ds$ and $K^- * v := \int_0^\infty K(s)v(x-s)\,ds$. The linear operator $\mathcal{L}$ associated with system (10) can be rewritten as $\mathcal{L} = \mathcal{L}_0 - \gamma\mathcal{L}_d$, where $\mathcal{L}_d$ is the differential operator $\mathcal{L}_d(u_1^+, u_1^-)^T = \mathrm{diag}(\partial_x, -\partial_x)(u_1^+, u_1^-)^T$, and

$$\mathcal{L}_0 \begin{pmatrix} u_1^+ \\ u_1^- \end{pmatrix} = \begin{pmatrix} -L_1 + R_2 K^- * \cdot & L_1 - R_2 K^+ * \cdot \\ L_1 - R_2 K^- * \cdot & -L_1 + R_2 K^+ * \cdot \end{pmatrix} \begin{pmatrix} u_1^+ \\ u_1^- \end{pmatrix}, \tag{11}$$

with $R_2 = 2R_1 u^*$. Consider now the linearized system (10) written as an abstract differential equation

$$\partial_t u = \mathcal{L}(u, \mu), \tag{12}$$

with μ a vector of parameters. Because $\mathcal{L}_0$ is a bounded operator on $L^p([0,L], \mathbb{R}^2)$, using a result from Hillen [26] (Theorem 3.4), it can be shown that the linear operator $\mathcal{L}$ with domain

$$X := \{u = (u^+, u^-) \in W^{1,p}([0,L], \mathbb{R}^2) \mid u^\pm(0) = u^\pm(L_0)\}$$

generates a strongly continuous semigroup on $L^p([0,L], \mathbb{R}^2)$. We now use X as the phase space to (12). Since we consider an equilibrium with isotropy subgroup $\mathbf{O}(\mathbf{2})$, there is an action of $\mathbf{O}(\mathbf{2})$ on X, given by (5) and (6). We can now write the isotypic decomposition of X. Let $k_n = 2\pi n/L$ and we decompose $u^\pm$ using Fourier series

$$u^\pm(x) = a_0^\pm + a_1^\pm e^{ik_1 x} + \cdots + a_n^\pm e^{ik_n x} + \cdots + \text{c.c.}$$

Here, $a_n^\pm \in \mathbb{C}$ and "c.c." stands for "complex conjugates".

Theorem 3.1 *For all $n \geq 1$, the subspaces*

$$X_n = \left\{ a e^{ik_n x} + c.c. \mid a = (a^+, a^-) \in \mathbb{C}^2 \right\} \subset X.$$

are isomorphic to $\mathbb{C}^2$, $\mathbf{O}(\mathbf{2})$-invariant, and can be decomposed as $X_n = X_n^1 \oplus X_n^2$. This decomposition is defined as follows. Given $f_1 = (1,1)^T$ and $f_2 = (1,-1)^T$, then

$$X_n^1 = \{(v_0 e^{ik_n x} + \overline{v}_0 e^{-ik_n x}) f_1 \mid v_0 \in \mathbb{C}\} \quad \textit{and} \quad X_n^2 = \{(v_1 e^{ik_n x} + \overline{v}_1 e^{-ik_n x}) f_2 \mid v_1 \in \mathbb{C}\} \tag{13}$$

are real two-dimensional $\mathbf{O}(\mathbf{2})$-irreducible representations (written in complex notation). The action (5) and (6) induces the following action on $\mathbb{C}^2$:

$$\theta.(v_0, v_1) = (e^{k_n i\theta} v_0, e^{k_n i\theta} v_1) \quad \textit{and} \quad \kappa.(v_0, v_1) = (\overline{v}_0, -\overline{v}_1). \tag{14}$$

Proof: The subspaces

$$V_n = \left\{ z e^{ik_n x} + \text{c.c.} \mid z \in \mathbb{C} \right\}$$

are invariant with respect to the $\mathbf{SO}(2)$ action (5), since the translation $x \to x + \theta$ acts on elements of V_n as

$$z e^{ik_n x} + \text{c.c.} \to z e^{ik_n (x+\theta)} + \text{c.c} = (z e^{ik_n \theta}) e^{ik_n x} + \text{c.c.} \tag{15}$$

This induces the action $z \to e^{ik_n \theta} z$ on $\mathbb{C}$. Moreover, the κ-action (6) leaves X_n invariant:

$$\kappa. \begin{pmatrix} a^+ \\ a^- \end{pmatrix} e^{ik_n x} + \text{c.c.} = \begin{pmatrix} a^- \\ a^+ \end{pmatrix} e^{ik_n (L-x)} + \text{c.c.} = \begin{pmatrix} \overline{a^-} \\ \overline{a^+} \end{pmatrix} e^{ik_n x} + \text{c.c.}.$$

Thus, X_n is $\mathbf{O}(2)$-invariant, but it is not irreducible. It is straightforward to check that X_n can be decomposed into a sum of isomorphic $\mathbf{O}(\mathbf{2})$ irreducible representations X_n^1 and X_n^2 given by (13). Thus, X_n is parametrized by $(v_0, v_1) \in \mathbb{C}^2$, with the action given by (14). ∎

The subspaces X_n are called isotypic components of the isotypic decomposition of X. By the $\mathbf{O}(\mathbf{2})$-equivariance of $\mathcal{L}$, each X_n is $\mathcal{L}$-invariant and one can restrict $\mathcal{L}$ along each isotypic component X_n. We now obtain the decomposition of $\mathcal{L}$ along the isotypic decomposition X_n: $\mathcal{L}_n := \mathcal{L}|_{X_n}$. To compute $\mathcal{L}_n$ explicitly, we let $\hat{K}^+(k_n) := \int_0^\infty K(s) e^{ik_n s}\, ds$ and so

$$\begin{aligned} &K^+ * e^{ik_n x} = \hat{K}^+(k_n) e^{ik_n x},\ K^- * e^{ik_n x} = \overline{\hat{K}^+(k_n)} e^{ik_n x}, \\ &K^+ * e^{-ik_n x} = \overline{\hat{K}^+(k_n)} e^{-ik_n x},\ K^- * e^{-ik_n x} = \hat{K}^+(k_n) e^{-ik_n x}. \end{aligned}$$

We obtain

$$\mathcal{L}(v_0 e^{ik_n x} f_1) = \left(R_2(\overline{\hat{K}^+(k_n)} - \hat{K}^+(k_n)) - \gamma i k_n \right) v_0 e^{ik_n x} f_2,$$

$$\mathcal{L}(v_1 e^{ik_n x} f_2) = -\gamma i k_n v_1 e^{ik_n x} f_1 + \left(-2L_1 + R_2(\hat{K}^+(k_n) + \overline{\hat{K}^+(k_n)}) \right) v_1 e^{ik_n x} f_2.$$

Therefore, for $a_1, a_2 \in \mathbb{C}$,

$$\mathcal{L}_n \begin{pmatrix} a_1 \\ a_2 \end{pmatrix} e^{ik_n x} = \begin{pmatrix} 0 & -ik_n\gamma \\ R_2(\overline{\hat{K}^+(k_n)} - \hat{K}^+(k_n)) - ik_n\gamma & -2L_1 + R_2(\hat{K}^+(k_n) + \overline{\hat{K}^+(k_n)}) \end{pmatrix} \begin{pmatrix} a_1 \\ a_2 \end{pmatrix} e^{ik_n x}. \tag{16}$$

3.1.1 Critical eigenvalues of $\mathcal{L}_n$ and dispersion relations

The eigenvalues of $\mathcal{L}_n$ are

$$\sigma_\pm(k_n) = -(L_1 - R_2 \text{Re}(\hat{K}^+(k_n))) \pm \sqrt{(L_1 - R_2 \text{Re}(\hat{K}^+(k_n)))^2 - (k_n^2\gamma^2 - 2R_2 k_n \gamma \text{Im}(\hat{K}^+(k_n)))}. \tag{17}$$

Note that the matrix in (16) has an eigenvalue $\sigma = 0$ if $R_2(\overline{\hat{K}^+(k_n)} - \hat{K}^+(k_n)) - ik_n\gamma = 0$. The corresponding eigenspace is $\mathbb{C}\{(1,0)^T\}$. For $\sigma = i\omega$, the non-trivial solution of

$$\begin{pmatrix} i\omega & ik_n\gamma \\ -R_2(\overline{\hat{K}^+(k_n)} - \hat{K}^+(k_n)) + ik_n\gamma & i\omega + (2L_1 - R_2(\hat{K}^+(k_n) + \overline{\hat{K}^+(k_n)})) \end{pmatrix} \begin{pmatrix} a_1 \\ a_2 \end{pmatrix} = 0$$

leads to $\omega a_1 + k_n\gamma a_2 = 0$, and so the eigenspace is $\mathbb{C}\{(k_n\gamma, -\omega)^T\}$.

The linear analysis above is equivalent to computing the dispersion relation, which is obtained by substituting

$$u^+ = u^* + a_1 e^{\sigma t + k_n x i}, \qquad u^- = u^* + a_2 e^{\sigma t + k_n x i},$$

into $\partial_t u = \mathcal{L}u$. After simplification, this can be rewritten as a matrix-vector product

$$\begin{pmatrix} \sigma + ik_n\gamma + L_1 - R_2\overline{\hat{K}^+(k_n)} & -L_1 + R_2\hat{K}^+(k_n) \\ -L_1 + R_2\overline{\hat{K}^+(k_n)} & \sigma - k_n i\gamma + L_1 - R_2\hat{K}^+(k_n) \end{pmatrix} \begin{pmatrix} a_1 \\ a_2 \end{pmatrix} = 0. \tag{18}$$

The previous equation has a nonzero solution if the determinant of the matrix is zero, that is

$$\sigma^2 + 2(L_1 - R_2\mathrm{Re}(\hat{K}^+(k_n)))\sigma + (k_n^2\gamma^2 - 2k_n\gamma R_2\mathrm{Im}(\hat{K}^+(k_n))) = 0. \tag{19}$$

Equation (19) is the dispersion relation. The roots of this equation (i.e., the eigenvalues) are given by (17).

If one considers the total population density A as a parameter of the system, then this parameter enters the eigenvalues through the term $R_2 = 2R_1u^*$, where $u^* = A/2$. The following results investigate the stability of the spatially homogeneous equilibrium as R_2 (and implicitly A) is varied.

Proposition 3.2 *Suppose that q_r, q_a and q_{al} are fixed, and consider the parabola given by*

$$P_n := \mathrm{Re}(\hat{K}^+(k_n))R_2^2 + (2k_n\gamma\mathrm{Im}(\hat{K}^+(k_n)) - 2L_1\mathrm{Re}(\hat{K}^+(k_n)))R_2 + (L_1^2 - k_n^2\gamma^2).$$

Then, the equilibrium with isotropy subgroup $\mathbf{O(2)}$ is asymptotically stable if and only if for all $n \in \mathbb{N}$, either

(1) $P_n \leq 0$ and $R_2\mathrm{Re}(\hat{K}^+(k_n)) < L_1$, or

(2) $P_n > 0$ and $2R_2\mathrm{Im}(\hat{K}^+(k_n)) < k_n\gamma$.

The first set of inequalities corresponds to the case of a complex eigenvalue with non-zero imaginary part and negative real part, while the second set of inequalities corresponds to real negative eigenvalues.

Proof: Write (17) as $\sigma_\pm = \alpha_n \pm \sqrt{\alpha_n^2 - 4\beta_n}$. Define $P_n = \alpha_n^2 - 4\beta_n$. If $P_n \leq 0$, then $\sigma_\pm$ has a nonzero imaginary part. The real part of $\sigma_\pm$ is negative if $\alpha_n < 0$. This inequality can be rewritten as $R_2\mathrm{Re}(\hat{K}^+(k_n)) < L_1$. If $P_n > 0$, then σ_+ is negative when $\beta_n > 0$, and this can be rewritten as $2R_2\mathrm{Im}(\hat{K}^+(k_n)) < k_n\gamma$. ∎

We now analyze the spectrum of (1) for a fixed domain size L. One can verify that for $R_2 = 0$, the conditions of Proposition 3.2 are satisfied and the equilibrium at the origin is asymptotically stable. As R_2 is increased from 0, there exists a critical value R_2^* for which the inequality conditions in Proposition 3.2 are not satisfied for a first value of $n \in \mathbb{N}$. Therefore, the equilibrium with isotropy subgroup $\mathbf{O(2)}$ generically loses stability to either a steady-state pattern or a periodic pattern. This is summarized in the following.

Corollary 3.3 *For fixed values of q_r, q_a and q_{al}, there exists a value $R_2^* > 0$ for which at least one eigenvalue σ of the equilibrium solution with isotropy subgroup $\mathbf{O(2)}$ crosses the imaginary axis with nonzero speed.*

This shows that for a given species with fixed social behaviour parameters, aggregation patterns can emerge in a fixed domain if the total population density increases beyond a threshold at which equal left- and right-moving homogeneous distributions are no longer sustainable. Density dependent patterning is seen, for instance, in locust aggregation outbreaks [6, 46].

For the remainder of the paper, we consider the total population A to be fixed and the bifurcation parameters to be q_r and q_a. Since we are working on finite domains $[0, L]$, the wave numbers k_j that appear in the dispersion relation (19) and the eigenvalues (17) are discrete.

4 Codimension-two bifurcations

In this section, we show the existence of codimension-two bifurcations, and calculate the linear terms at the bifurcation and the eigenfunctions of the bifurcating solutions. Since near a bifurcation point, the eigenfunctions give an approximation to the bifurcating solutions, we create plots of these eigenfunctions. Then, we use these plots as a guide for classifying solutions obtained via numerical simulations of (1) near the codimension-two points. In particular, fine details in the plots of the eigenfunctions are useful for identifying the isotropy subgroups of numerical solutions. Moreover, numerical simulations with initial conditions close to the bifurcation point often evolve towards several intermediate unstable states before settling into a seemingly asymptotically stable solution which may not be close to the bifurcation point. Using the eigenfunction plot as comparison, one can speculate on the unstable states visited.

The section is structured as follows. We begin by identifying the presence of codimension-two points. Then, in Section 4.1, we obtain explicit expressions for the solutions of the linear system near the codimension-two points along with the $\mathbf{O(2)}$ group actions on the respective eigenspaces. Section 4.2 looks in detail at the orbit representatives of solutions with isotropy subgroups for the SS/H. We present numerical simulations near the SS/H point and use the plots of eigenfunctions to proceed to a possible classification of the states obtained. A similar investigation is performed in Section 4.3, near the SS/SS point.

The graphical linear stability analysis below reveals that model (1) can exhibit three types of codimension-two bifurcations: Hopf/Hopf, Steady-state/Hopf and Steady-state/Steady-state bifurcations. These codimension-two points are obtained by studying the intersection between different neutral stability curves (that is, curves described by $\mathrm{Re}\big(\sigma(k_n)\big) = 0$). Figures 3 (a) and (c) show the neutral stability curves corresponding to various modes k_n, $n = 1, \ldots, 14$, as two

parameters, q_a and q_r are varied. For $q_{al} = 0$ (Figure 3(a)), we identify the 3:4 H/H point (located near $(q_a, q_r) = (0.64, 3.61)$) as well as the 1:4 SS/H point (located near $(q_a, q_r) = (1.56, 2.71)$). For $q_{al} = 3$ (Figure 3(c)) we identify the 13:14 SS/SS point (located near $(q_a, q_r) = (1.02, 1.02)$). All these codimension-two bifurcation points are at the boundary of the stability region for the $\mathbf{O(2)}$-symmetric steady-state. The hatched areas show the stability regions for each of these cases. Figures 3 (b) and (d) show the real and imaginary parts of the dispersion relations corresponding to each of the wave numbers involved in the H/H, H/S and SS/SS bifurcations.

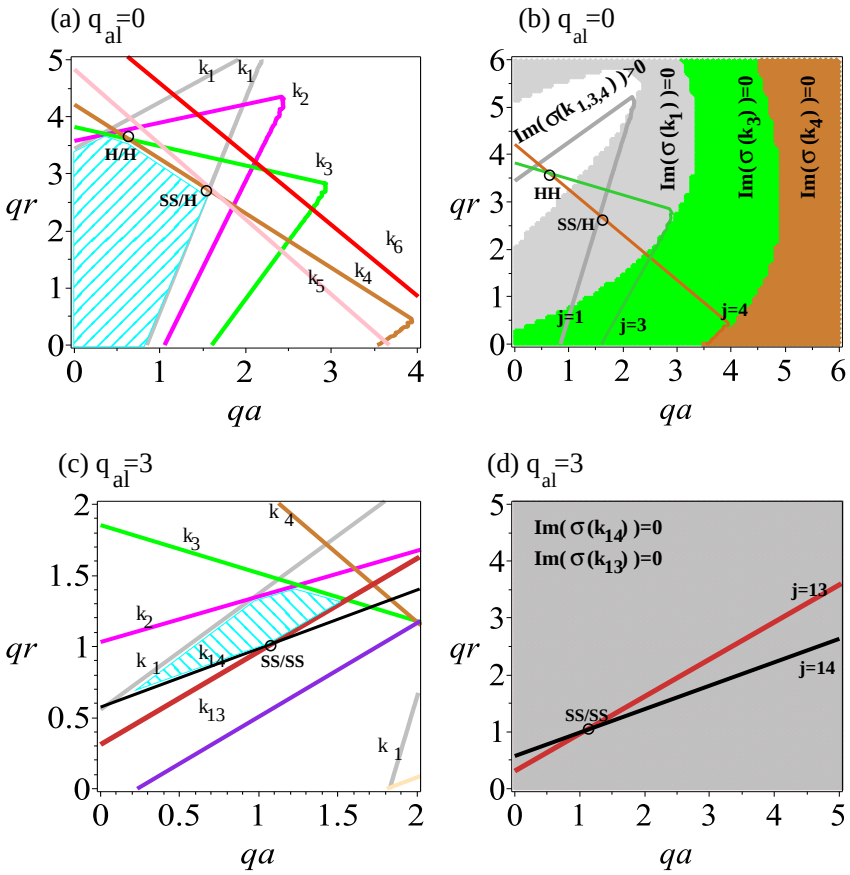

Figure 3: (a) Real parts of the dispersion relation $\sigma(k_n)$ corresponding to wave numbers k_n, $n = 1, \ldots, 6$, as two parameters, q_r and q_a, are varied. The hatched area shows the stability region. (b) The $n = 1$, $n = 3$ and $n = 4$ neutral stability curves. The shaded areas show the region where $\mathrm{Im}(\sigma(k_n)) = 0$, $n = 1, 3, 4$. (c) is similar to (a), but for $q_{al} = 3$. The SS/SS point is at the intersection of k_{13} and k_{14}. The hatched area shows the stability region. (d) is similar to (b) but for $q_{al} = 3$. The shaded area corresponds to $\mathrm{Im}(\sigma(k_{13})) = \mathrm{Im}(\sigma(k_{14})) = 0$.

Since the stability curves corresponding to various modes are sometimes very close to each other, it is possible to have multiple mode interactions, which may influence the final patterns. One such example is given by the SS/H bifurcation (Figure 3 (a)), where the intersection point between k_1 and k_4 is very close to the intersection point between k_4 and k_5. This can be seen

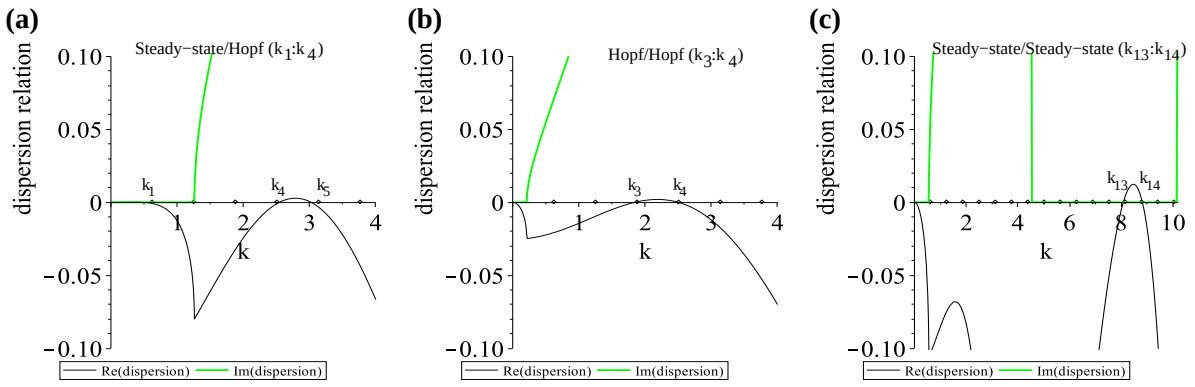

Figure 4: Real and imaginary parts for the dispersion relation $\sigma(k_n)$, for different wave numbers and different parameter ranges, as two parameters, q_r and q_a, are varied. (a) Steady-state/Hopf bifurcation for $q_{al} = 0$, $q_a = 1.56$, $q_r = 2.71$, $\lambda_1 = 0.2$, $\lambda_2 = 0.9$. The modes that become first unstable are k_1 (Steady state) and k_4 (Hopf). (b) Hopf/Hopf bifurcation for $q_{al} = 0$, $q_a = 0.64$, $q_r = 3.61$, $\lambda_1 = 0.2$, $\lambda_2 = 0.9$. The modes that become first unstable are k_3 and k_4. (c) Steady-state/Steady-state bifurcation for $q_{al} = 3.0$, $q_a = 1.02$, $q_r = 1.02$, $\lambda_1 = 0.2/0.29$, $\lambda_2 = 0.9/0.29$. The modes that become first unstable are k_{13} and k_{14}.

more clearly in Figure 4, which shows the real and imaginary parts of the dispersion relation $\sigma(k_n)$, as functions of the wave numbers k_n, $n > 0$. For the SS/H bifurcation (Figure 4(a)), the curve that passes through k_1 and k_4 is also very close to k_5. This may lead to more complex spatial and spatio-temporal patterns.

4.1 Linear modes at bifurcation

Consider the linear system

$$\partial_t U(x,t) = \mathcal{L}_n U(x,t), \tag{20}$$

where $U(x,t) = (u^+(x,t), u^-(x,t))$. Using the basis $\{f_1, f_2\}$, we can write the solutions

$$U(x,t) = \mathrm{Re}\left(\begin{pmatrix} v_0 \\ v_1 \end{pmatrix} e^{ik_n x} e^{\sigma t} \right) = \mathrm{Re}(v_0 e^{ik_n x} e^{\sigma t}) f_1 + \mathrm{Re}(v_1 e^{ik_n x} e^{\sigma t}) f_2.$$

As seen in Section 3.1.1, the eigenvalue $\sigma = 0$ has the eigenspace $\mathbb{C}\{(1,0)^T\}$, and therefore

$$U(x,t) = \mathrm{Re}(v_0 e^{ik_n x}) f_1.$$

For $\sigma = \pm i\omega$, the eigenspaces are $\mathbb{C}\{(k_n\gamma, -\omega)^T\}$ and $\mathbb{C}\{(k_n\gamma, \omega)^T\}$, respectively. Letting $\Phi_1^n = k_n\gamma f_1$ and $\Phi_2 = -\omega f_2$, solutions of the linear system (20) can be written as

$$U(x,t) = \mathrm{Re}(w_1 e^{ik_n x} e^{i\omega t})(\Phi_1^n + \Phi_2) + \mathrm{Re}(w_2 e^{ik_n x} e^{-i\omega t})(\Phi_1^n - \Phi_2).$$

$\mathbf{O(2)}$ has the following action: $\kappa.(\Phi_1^n + \Phi_2) = \Phi_1^n - \Phi_2$, and θ acts trivially on Φ_1^n and Φ_2. Therefore, we can rewrite $U(x,t)$ as follows:

$$U(x,t) = w_1 e^{i\omega_1 t}(e^{ik_n x}(\Phi_1^n + \Phi_2)) + \overline{w_2} e^{i\omega_1 t}(e^{-ik_n x}(\Phi_1^n - \Phi_2)) + \text{c.c.}.$$

Now, we consider a new basis given by $\{h_1^n, h_2^n\} = \{e^{ik_n x}(\Phi_1^n + \Phi_2), e^{-ik_n x}(\Phi_1^n - \Phi_2)\}$. The action of $\mathbf{O(2)}$ on the elements of this basis is

$$\kappa.h_1^n = h_2^n, \quad \theta.h_1^n = e^{ik_n\theta}h_1^n \quad \text{and} \quad \theta.h_2^n = e^{-ik_n\theta}h_2^n.$$

This basis is the standard one, see [19], for the classification of isotropy subgroups in the $\mathbf{O(2)}$ Hopf bifurcation. The general real solution, which spans the generalised eigenspaces at the mode interaction points, can be obtained from the solutions of (20) for eigenvalues $\sigma = 0$ and $\sigma = i\omega$. At the $1:4$ SS/H point, we have

$$U(x,t) = \mathrm{Re}(z_0 e^{ik_1 x})f_1 + z_1 e^{i\omega t}h_1^4 + z_2 e^{i\omega t}h_2^4 + \text{c.c.}, \tag{21}$$

and the group action on (z_0, z_1, z_2) is

$$\begin{aligned} \theta.(z_0, z_1, z_2) &= (e^{ik_1\theta}z_0, e^{ik_4\theta}z_1, e^{-ik_4\theta}z_2), \\ \kappa.(z_0, z_1, z_2) &= (\overline{z}_0, z_2, z_1). \end{aligned} \tag{22}$$

The complex eigenvalue $i\omega$ generates an additional $\mathbf{S}^1$ symmetry on the critical eigenspace: $\psi.(z_0, z_1, z_2) = (z_0, e^{ik_4\psi}z_1, e^{ik_4\psi}z_2)$. The general real solution at the $3:4$ H/H bifurcation point is therefore

$$U(x,t) = (z_1 h_1^3 + z_2 h_2^3)e^{i\omega_1 t} + (z_3 h_1^4 + z_4 h_2^4)e^{i\omega_2 t} + \text{c.c.} \tag{23}$$

The action of $\mathbf{O(2)}$ on (z_1, z_2, z_3, z_4) is

$$\begin{aligned} \theta.(z_1, z_2, z_3, z_4) &= (e^{ik_3\theta}z_1, e^{-ik_3\theta}z_2, e^{ik_4\theta}z_3, e^{-ik_4\theta}z_4), \\ \kappa.(z_1, z_2, z_3, z_4) &= (z_2, z_1, z_4, z_3). \end{aligned} \tag{24}$$

The frequencies at the Hopf/Hopf bifurcation point are estimated to be $\omega_3 \approx 0.2461539166$ and $\omega_4 \approx 0.3454406196$, and therefore it is safe to assume that they are not rationally dependent. Therefore a $\mathbf{T}^2 = \mathbf{S}^1 \times \mathbf{S}^1$ action generated (after a convenient rescaling) by $e^{(ik_1/\omega_3)\psi_1\omega_3} \oplus e^{(ik_1/\omega_4)\psi_2\omega_4}$, with $\psi_1, \psi_2 \in [0, L)$, acts on the critical eigenspace $\mathbb{C}^2 \oplus \mathbb{C}^2$ as follows:

$$(\psi_1, \psi_2).(z_1, z_2, z_3, z_4) = (e^{ik_1\psi_1}z_1, e^{ik_1\psi_1}z_2, e^{ik_1\psi_2}z_3, e^{ik_1\psi_2}z_4). \tag{25}$$

Together, (24) and (25) generate the action of $\mathbf{O(2)} \times \mathbf{T}^2$ on the critical eigenspace and implicitly on the linear patterns given by $U(x,t)$. Finally, at the $13:14$ SS/SS point we have

$$U(x,t) = \mathrm{Re}(w_0 e^{ik_{13}x})f_1 + \mathrm{Re}(w_1 e^{ik_{14}x})f_1. \tag{26}$$

The classification of solutions in the H/H mode interaction is studied in greater details in [7] (which includes also a weakly-nonlinear analysis of the bifurcation patterns). The SS/H and SS/SS mode interactions are investigated below.

4.2 Study of the $1:4$ SS/H linear modes

Using equation (21), we obtain expressions for the primary bifurcating solutions at the $1:4$ SS/H mode interaction. These solutions are: (a) stationary pulses (SP) which are spatially heterogeneous steady-state solutions, (b) rotating wave periodic solutions (RW), and (c) standing wave periodic solutions (SW). The isotropy subgroups and orbit representatives for these bifurcating solutions are shown in Table 2 (see Hill and Stewart [25] for details). In the following, we give the analytical expressions for each of these solutions. Let $Z^{(\theta,\psi)}$ be the discrete subgroup

Isotropy subgroup	Orbit representative	Type
$\mathbf{O(2)} \times \mathbf{S}^1$	$(0,0,0)$	homogeneous steady-state
$\mathbb{Z}_2(\kappa) \times \mathbf{S}^1$	$(a,0,0)$	stationary pulse (SP)
$\widetilde{\mathbf{SO}}(2)$	$(0,b,0)$	rotating wave (RW)
$\mathbb{Z}_2(\kappa) \times Z^{(\pi/4,\pi)}$	$(0,b,b)$	standing wave (SW).

Table 2: Isotropy subgroups, orbit representatives and type of the primary bifurcating solutions on the centre manifold at a SS/H bifurcation (as described in Golubitsky *et al.* [19]), where $a, b \in \mathbb{R}$.

generated by $(\theta,\psi) \in \mathbf{O(2)} \times \mathbf{S}^1$. The cyclic group $Z^{(\pi/4,\pi)}$ has order eight, and its action on $U(x,t)$ is given by $(L/8, \pi/\omega)$, where $L/8$ is half the length of one fundamental domain in $[0,L]$ under the partition by the elements of the kernel of the $\mathbf{SO}(2)$ action. Using the orbit representatives in Table 2, we obtain the linear solutions for the primary bifurcating solution branches, and the total density $u(x,t) = u^+(x,t) + u^-(x,t)$ in each case. For example, in the case of the rotating wave (corresponding to the $\widetilde{\mathbf{SO}}(2)$ subgroup), because the spatial translation corresponds to phase shift on the periodic solution, the period is linked with the wave number. The rotating wave is fixed by $(\phi, -4\phi)$, and therefore

$$(\phi,-4\phi).U(x,t) = be^{i\omega(t-4\phi)}e^{ik_4 x}h_1^4 + \text{c.c.} = U(x,t)$$

requires that $\omega = 2\pi/L$. For the complete list of primary bifurcating solutions, see Table 3. To help the reader identify these solutions, and for further comparison with the results of the numerical simulations, we show these solutions in Figure 5, for some arbitrary parameter values: $\gamma = 1$, $a = 3$, $b = 1.3$, $\omega = 0.5$ and $L = 10$.

We also look for solutions with submaximal isotropy subgroups with fixed point subspaces of dimension three, namely $\mathbb{Z}_2(\kappa)$ and $\mathbb{Z}_2(\kappa L/8, \pi/\omega)$. The solutions corresponding to these subgroups are shown in Table 4. Again, to help the reader identify these solutions, we show them in Figure 6, for some arbitrary parameter values: $\gamma = 1$, $a = 3$, $b = 1.3$, $\omega = 0.5$ and $L = 10$. Close inspection of the contour plots in Figure 6(a) shows the solution $\mathbb{Z}_2(\kappa)$ with the reflection line for the symmetry κ near $x = 5$ (i.e., the white ellipses inside the red patterns are larger at $x \approx 5$, hence the density is slightly higher at this point). In Figure 6(b), the solution with isotropy subgroup $\mathbb{Z}_2(\kappa L/8, \pi/\omega)$ has eight reflection symmetries with vertical axes near

Isotropy subgroup	$U(x,t)$	$u(x,t)$
$\mathbb{Z}_2(\kappa)\times\mathbf{S}^1$	$\mathrm{Re}(ae^{ik_1x})f_1$	$2\mathrm{Re}(ae^{ik_1x})$
$\widetilde{\mathbf{SO}}(2)$	$be^{ik_1t}h_1^4+\text{c.c.}$	$2k_4\gamma be^{ik_1t}e^{ik_4x}+\text{c.c.}$
$\mathbb{Z}_2(\kappa)\times Z^{(\pi/4,\pi)}$	$be^{i\omega t}h_1^4+be^{i\omega t}h_2^4+\text{c.c.}$	$4k_4\gamma be^{i\omega t}\cos(k_4x)+\text{c.c.}$

Table 3: Maximal isotropy subgroups with representative solutions $U(x,t)$ and total density $u(x,t)$. For the $\widetilde{\mathbf{SO}}(2)$ solution $\omega=k_1$ is forced by symmetry.

$x=3+1.25j$, $j=0,\ldots,7$. Reflection across any of those vertical lines along with a time-shift by a half-period (corresponding to one row of cells) leaves the pattern unchanged.

Isotropy subgroup	$U(x,t)$	$u(x,t)$
$\mathbb{Z}_2(\kappa)$	$\mathrm{Re}(ae^{ik_1x})f_1+be^{i\omega t}(h_1^4+h_2^4)+\text{c.c.}$	$2\mathrm{Re}(ae^{ik_1x})+4k_4\gamma be^{i\omega t}\cos(k_4x)+\text{c.c.}$
$\mathbb{Z}_2(\frac{\kappa L}{8},\frac{\pi}{\omega})$	$\mathrm{Re}(ia'e^{ik_1x})f_1+be^{i\omega t}(h_1^4+h_2^4)+\text{c.c.}$	$2\mathrm{Re}(ia'e^{ik_1x})+4k_4\gamma be^{i\omega t}\cos(k_4x)+\text{c.c.}$

Table 4: Submaximal isotropy subgroups with representative solutions $U(x,t)$ and total density $u(x,t)$.

Comparison with numerical simulations Numerically simulated patterns of (1) that emerge around the SS/H bifurcation point are compared with the contour plots of the eigenfunctions obtained previously. The initial conditions for the numerical simulations are random perturbations of the spatially homogeneous steady states $u^{\pm}=u_3^*=1$. Figure 7 shows the spatial and spatio-temporal patterns that emerge at some randomly-chosen points (1)-(10) located around the $1:4$ SS/H point (see also Figures 3(a),(b) and Figure 4(a)). At points (1), (2), (3), (4), (9), (10), the small random perturbations of $u_3^*=1$ first evolve to standing wave patterns (panel (b)). These patterns are generally unstable, and after a while they evolve to quasi-periodic solutions (panel (e)) or to rotating waves (panel (f)). Both types of patterns seem stable (at least for $t\leq 4000$).

At points (5) and (6), the small perturbations of u_3^* lead to the emergence of stationary pulses. These stationary pulses are unstable and further evolve into the quasi periodic solutions shown in panel (e). However, at point (6), we observed that the stationary pulse first evolves into a pulse pattern with $\mathbb{Z}_2(\kappa)$ symmetry (panel (d)). Finally, at points (7) and (8), the spatially homogeneous solutions u_3^* are stable, and the perturbations which initially lead to modulated standing wave (MSW) patterns (panel (g)) eventually evolve towards the steady state u_3^* (panel (h)).

We remark here that the solutions with the submaximal isotropy subgroups $\mathbb{Z}_2(\kappa)$ and

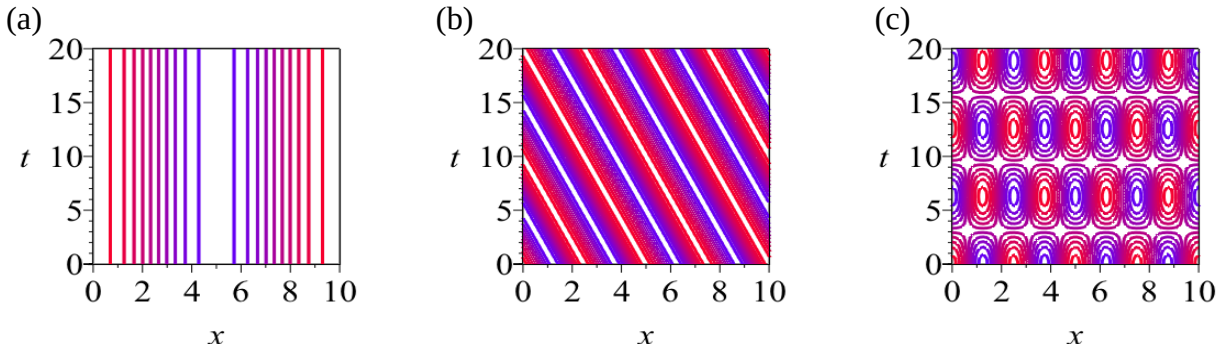

Figure 5: (a) Contour lines of $u(x,t)$ corresponding to the stationary pulse with isotropy subgroup $\mathbb{Z}_2 \times \mathbf{S}^1$ and wavenumber k_1. (b) Contour lines of $u(x,t)$ corresponding to the rotating wave with wavenumber k_4. (c) Contour lines of $u(x,t)$ corresponding to the standing wave with wavenumber k_4. To obtain these contour lines we choose the length of the domain $L = 10$. The rest of the parameters are $\gamma = 1$, $a = 3$, $b = 1.3$, $\omega = 0.5$.

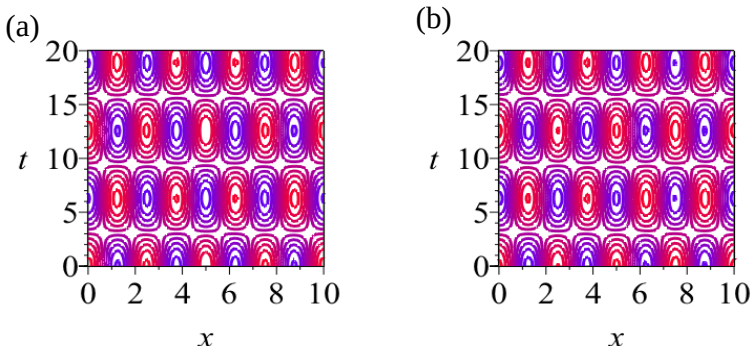

Figure 6: Contour lines of $u(x,t)$ for the solutions with submaximal isotropy subgroup (a) $\mathbb{Z}_2(\kappa)$ (b) $\mathbb{Z}_2(\frac{\kappa L}{8}, \frac{\pi}{\omega})$. To obtain these contour lines we choose the length of the domain $L = 10$. The rest of the parameters are $\gamma = 1$, $a = 3$, $a' = 100$, $b = 1.3$, $\omega = 0.5$.

$\mathbb{Z}_2(\kappa L/8, \pi/\omega)$ are sometimes difficult to be distinguished numerically from each other and from the standing wave solutions. Figure 8 shows the surfaces (panels (a),(c)) and the contour lines (panels (b),(d)) for two solutions that seem very similar. However, closer inspection of the contour lines shows that the symmetry of the patterns is quite different. In panel (b), contour lines suggest a solution with isotropy subgroup $\mathbb{Z}_2(\kappa L/8, \pi/\omega)$, where the axes of symmetry are the vertical lines between neighboring cells, and the phase shift by a half-period seems to correspond to an upward shift by three-rows of cells. In panel (d), there are four translated copies of pairs of cells along the x-axis, and $x \approx 5$ is a reflection symmetry for the pattern; this suggests a standing wave. (Compare these patterns with the contour plots in Figure 6(b) and Figure 5(c)). Note that from the numerical simulations, these states are likely unstable and therefore the trajectory is bounded away from the actual state. This explains the fact that the patterns exhibit only

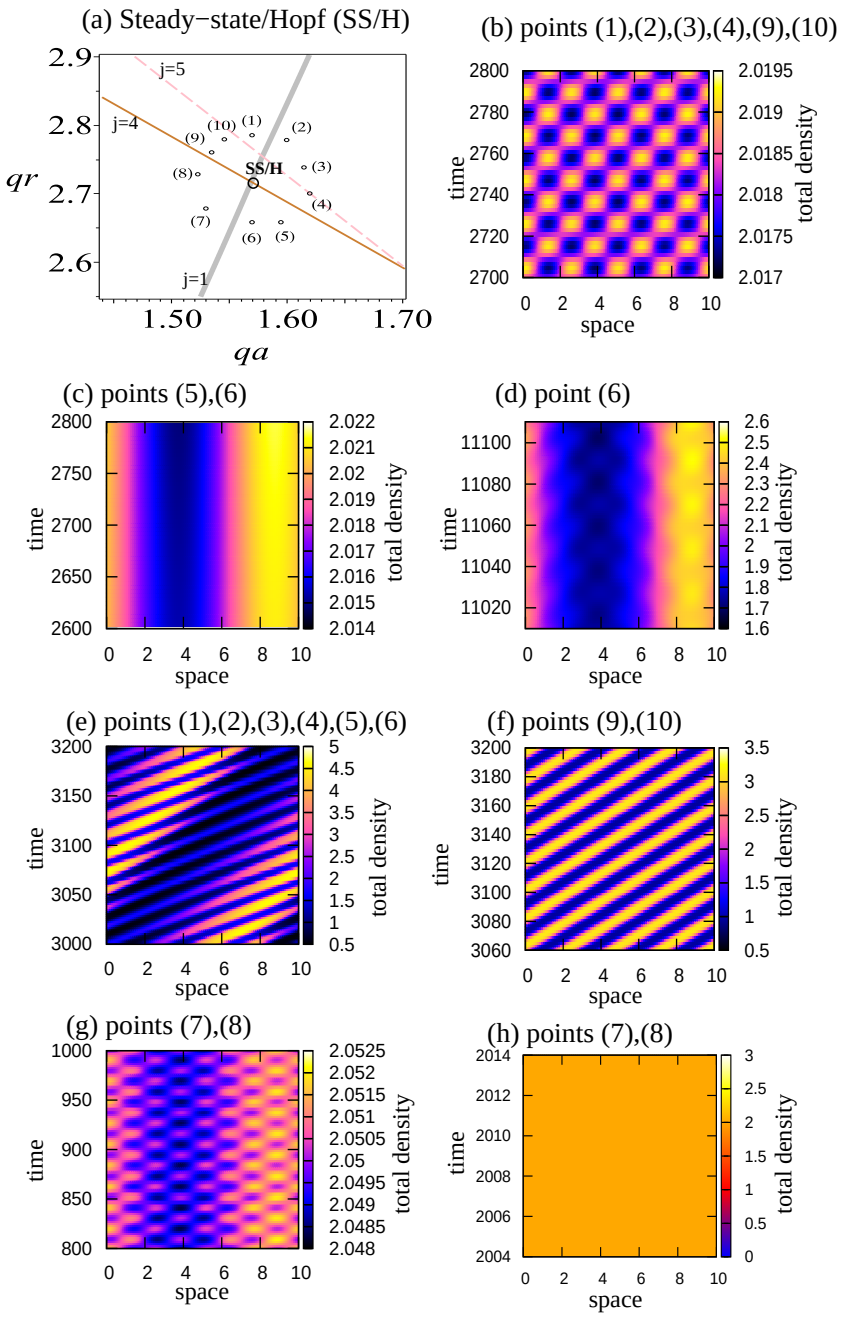

Figure 7: (a) Neutral stability curves for wave numbers k_1 and k_4. The points (1)-(10) are randomly chosen around the SS/H bifurcation point located at $(q_a, q_r) = (1.5686, 2.7178)$. (b) The patterns that emerge at points (1), (2), (3), (4), (9) and (10) all evolve first to standing waves. (c) The patterns that emerge at points (5),(6) evolve towards a spatially heterogeneous steady state (i.e., stationary pulse). (d) The stationary pattern at (6) first evolves into a pattern with $\mathbb{Z}_2(\kappa L/8, \pi/\omega)$ symmetry. (e) The patterns starting at (1),(2),(3),(4),(5) and (6) eventually evolve from standing waves and stationary solutions to quasi-periodic solutions. (f) The patterns starting at (9) and (10), after the excursion near a standing wave, eventually approach rotating wave solutions. (g) At points (7) and (8), small perturbations of the spatially homogeneous steady states evolve first to modulated standing waves, i.e., patterns with $\mathbb{Z}_2(\kappa L/8, \pi/\omega)$. (h) Since the points (7),(8) are in the parameter region where the spatially homogeneous solutions u_3^* are stable, no spatially heterogenous patterns can persist at these points, and thus the total density shown is $u_3^* + u_3^* = 2(= A)$. The parameters are: $q_{al} = 0.0$, $\lambda_1 = 0.2$, $\lambda_2 = 0.9$, $\gamma = 0.1$, $L = 10$.

approximate symmetries (see, for instance, the slight tilt of the cells, and the differences in some contour lines, shown more clearly in panel (b)). We expect that a numerical corrector method starting at these patterns should converge to the actual periodic solution. (Such a corrector is under construction [31].) In the following, we summarize the output suggested by the numerical

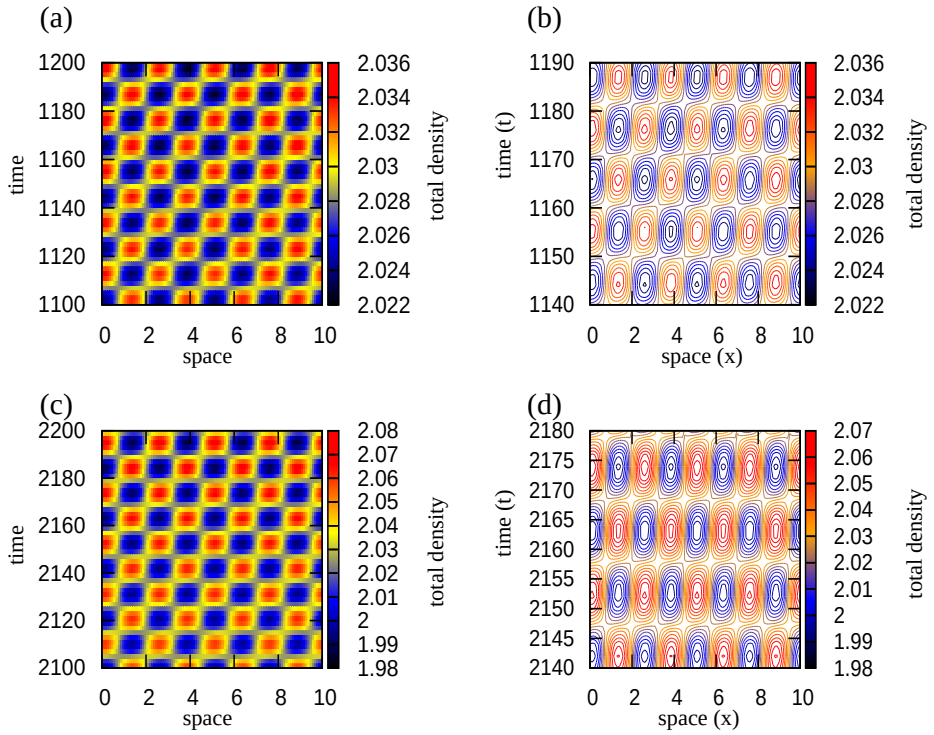

Figure 8: (a) Solution with submaximal isotropy subgroup $\mathbb{Z}_2(\kappa L/8, \pi/\omega)$; (b) Contour lines of $u(x,t)$ for the solution in panel (a); (c) Standing wave solution; (d) Contour lines of $u(x,t)$ for solution in panel (c). The parameters are: $q_{al} = 0.0$, $\lambda_1 = 0.2$, $\lambda_2 = 0.9$, $\gamma = 0.1$, $L = 10$, $A = 2$

simulations.

- The stationary pulse bifurcates supercritically. It is unstable at this parameter value.
- The standing wave and rotating wave bifurcate subcritically (so, they are unstable near bifurcation).
- RW and Modulated Rotating Wave (MRW) are observed to be asymptotically stable. MRW stable over a wide parameter range.
- $\mathbb{Z}_2$-symmetric periodic solutions are unstable and are observed in the region of asymptotic stability of the equilibrium.

- Note that panels (d) and (g) in Figure 7 have the same isotropy subgroup and may lie on a mixed-mode branch of periodic solutions connecting SP and SW.

We return to these features in Section 5, where we use them along with formal normal form analysis and weakly nonlinear analysis to propose a bifurcation diagram near the SS/H point.

4.3 $13:14$ SS/SS: linear modes

For the details of the analysis of the $\mathbf{O}(\mathbf{2})$ steady-state mode interaction, we refer the reader to [19], which investigates the case of interacting wavenumbers m and ℓ, with $m = \ell + 1$. In our case, $\ell = 13$ and $m = 14$. The orbit representatives for the fixed-point subspaces of the isotropy subgroups corresponding to the $\mathbf{O}(\mathbf{2})$ action on the critical eigenspace $\mathbb{C}^2$, can be found in [19](Chapter XX, Table 1.1). In the following, we write the eigenfunctions corresponding to each of these orbit representatives.

(a) The isotropy subgroups $\mathbf{D}_{13}$ and $\mathbf{D}_{14}$ have the orbit representatives (i) $w_0 = x_0$, $w_1 = 0$, and (ii) $w_0 = 0$, $w_1 = y_0$, respectively. The corresponding eigenfunctions are

$$\text{(i) } U(x,t) = \mathrm{Re}(x_0 e^{ik_{13}x}) f_1, \quad \text{(ii) } U(x,t) = \mathrm{Re}(y_0 e^{ik_{14}x}) f_1.$$

(b) The isotropy subgroup $\mathbb{Z}_2$ has the orbit representative $w_0 = x_0$, $w_1 = y_0$. The corresponding eigenfunction is

$$U(x,t) = \mathrm{Re}(x_0 e^{ik_{13}x}) f_1 + \mathrm{Re}(y_0 e^{ik_{14}x}) f_1.$$

The contourplots of $u(x,t) = u^+(x,t) + u^-(x,t)$ are shown in Figure 9(a,b). Figure 9(c) shows the contourplots of $u(x,t) = u^+(x,t) + u^-(x,t)$, for the mixed-mode interaction with wave numbers k_{13} and k_{14}.

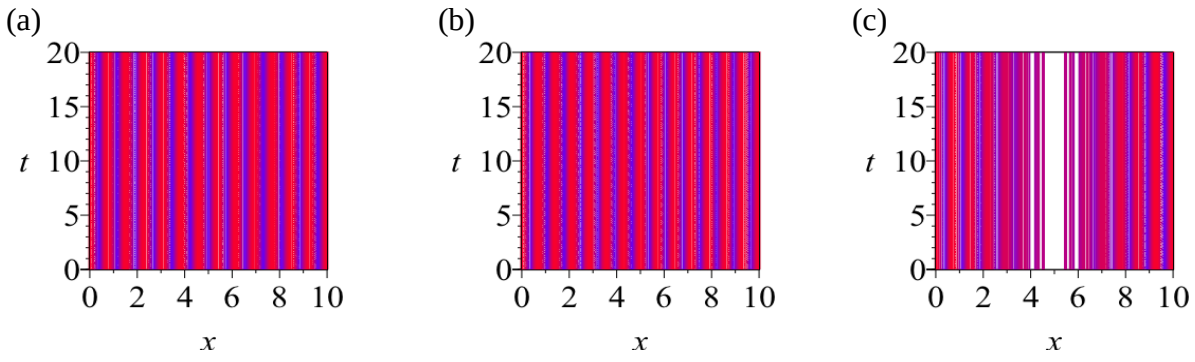

Figure 9: (a) and (b): Contour lines of $u(x,t)$ with isotropy subgroups $\mathbf{D}_{13}$ and $\mathbf{D}_{14}$, respectively. (c) Contour lines of $u(x,t)$ for the mixed mode solution with isotropy subgroup $\mathbb{Z}_2$ (with the same two modes as in panel (a) and (b)). To obtain these contour lines we choose the length of the domain $L = 10$.

Comparison with numerical simulations In the following, we include the alignment interaction ($q_{al} = 3 > 0$), and investigate the formation of patterns near a Steady-state/Steady-state (SS/SS) bifurcation point (see Figure 4(c)). Note that the SS/SS bifurcation can occur also for $q_{al} = 0$ (e.g., for $q_a = 0.2$, $q_r = 1$, $\lambda_1 = 0.2/0.06$, $\lambda_2 = 0.9/0.06$). However, in this case, the emergent wavenumbers are k_{28} and k_{29}, which makes it difficult to distinguish very clearly the spatial patterns (which now have 28 or 29 peaks). Moreover, the neutral stability curves for wavenumbers k_{28} and k_{29} are very close to the neutral stability curves for wavenumbers k_1 and k_{30}. This proximity influences the patterns (corresponding to k_{28} and k_{29}) that form near the codimension-two bifurcation point. For these reasons, we prefer to run simulations with $q_{al} > 0$.

Figure 10 shows the numerical patterns that emerge at various points around the SS/SS bifurcation located at $(q_a, q_r) = (1.02, 1.02)$. The initial conditions for the numerical simulations are small random perturbations of the spatially homogeneous steady-states $u^{\pm} = u_3^* = 1$. First, the points (8),(9),(1) are in the parameter region where the state $u_3^* = 1$ is stable, and hence no pattern can form (see panel (f), which depicts the difference $|u^+ - u^-| = u_3^* - u_3^* = 0$). At points (2)-(7), the unstable spatially homogeneous states u_3^* evolves initially to mixed-mode spatially heterogeneous solutions formed of 13 peaks (corresponding to wavenumber k_{13}). For the patterns at (3)-(7), as time progresses, one of the peaks then splits into two other peaks, thus giving rise to 14 peaks (corresponding to k_{14}). These mixed-mode patterns have the axis of symmetry near $x = 6$. At points (2),(3), these mixed-mode patterns then evolve into simple-mode patterns (panel (c)). At points (3),(5),(6), the patterns then approach a high-amplitude mixed-mode solution (panel (d)) with 14 peaks. The axis of symmetry of this mixed-mode solution is also near $x = 6$. The high-amplitude patterns in panel (d) seem to be asymptotically stable, while the patterns in panels (b),(c) are unstable and, for longer time integrations, evolve to other states.

Despite the fact that the points at (2),(7) are in the parameter region where k_{13} is unstable, the patterns eventually decay towards the spatially homogeneous steady state u_3^* (see panel (f)). This is likely an artifact of the numerical scheme (first order upwind scheme), combined with a lower amplitude of the dispersion relation at point (2). The pattern at (4), after approaching first an unstable high-amplitude solution similar to the one in panel (d), eventually evolves to the spatially homogeneous steady state $u_{1,5}^*$ (see panel (e), which depicts the difference $|u^+ - u^-|$ that approaches asymptotically the value $|u_1^* - u_5^*| = 1.44$).

Note that when $q_{al} = 0$ (and $q_a = 0.2$ $q_r = 1.0$), we would obtain similar spatial patterns around the SS/SS bifurcation point. However, since in this case attraction is much weaker than repulsion, the spatially heterogeneous solutions would be always decaying towards the spatially homogeneous steady states (either u_3^* or $u_{1,5}^*$; see Figure 10(e),(f)).

5 Bifurcation Diagrams

The bifurcation analysis near the Steady-state/Hopf bifurcation point is typically done using Centre Manifold Reduction (CMR) or Lyapunov-Schmidt Reduction (LSR). However, the unboundedness of the derivative operator along with the nonlocal nature of the turning function prevents the use of current versions of CMR and LSR. To be able to use CMR or LSR, one would

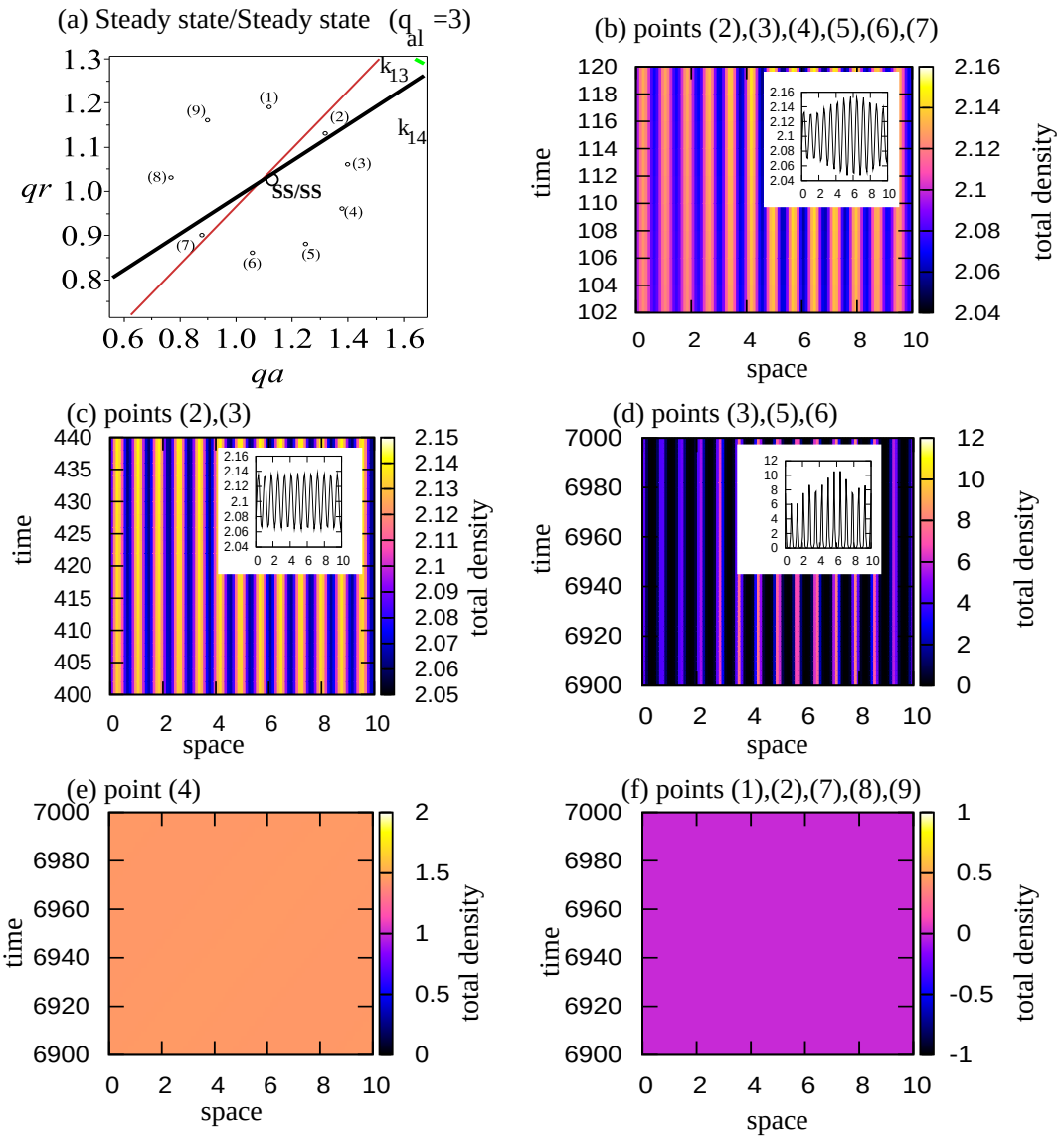

Figure 10: (a) Neutral stability curves for wave numbers k_{13} and k_{14}. The points (1)-(9) are randomly chosen around the SS/SS bifurcation point located at $(q_a, q_r) = (1.02, 1.02)$. Panels (b)-(d) show the the total density $u^+ + u^-$. Panels (e)-(f) show the difference $|u^+ - u^-|$. (b) The patterns that emerge at points (2)-(7) initially evolve towards an unstable mixed-mode spatially heterogeneous solution formed of 13 or 14 peaks. The inset shows the total density $u^+ + u^-$ at time $t = 120$. (c) The patterns that emerge at points (2), (3) then evolve towards simple-mode patterns. The inset shows the total density $u^+ + u^-$ at time $t = 400$. (d) The unstable solutions at points (3),(5) and (6) next evolve towards a stable mixed-mode solution with 14 peaks. The inset shows the total density $u^+ + u^-$ at time $t = 1400$. (e) The unstable solutions at points (4) and (7) evolve asymptotically towards the spatially homogeneous steady states $u^*_{1,5}$. Shown is the difference $|u^+ - u^-|$, which in the long term approaches $|u^*_1 - u^*_5| = 1.44$. (f) Since the points (1), (8), (9) are in the parameter region where the spatially homogeneous states u^*_3 are stable, no patterns can form. To distinguish this dynamics from the dynamics in panel (e), we show the difference $|u^+ - u^-|$ which approaches asymptotically the difference $|u^*_3 - u^*_3| = 0$. The parameters are: $q_{al} = 3.0$, $\lambda_1 = 0.2/0.29$, $\lambda_2 = 0.9/0.29$, $\gamma = 0.1$, $L = 10$.

need to show a spectral gap property for the linear system, or to show that the linear operator is Fredholm (of index 0). There does not seem to be any obstacle in proving such technical results. However, because of the complexity of the analysis, we leave this question to another paper. Instead, we perform a weakly-nonlinear analysis which provides amplitude equations for bounded solutions corresponding to critical eigendirections near the bifurcation point. In many cases, the resulting amplitude equations are equivalent to CMR and LSR [1, 15, 17].

5.1 Steady-state/Hopf: bifurcation analysis

Hill and Stewart [25] studied the Steady-State/Hopf bifurcation with $\mathbf{O(2)}$-symmetry. They assumed that a Lyapunov-Schmidt reduction has been applied to the equation

$$\frac{dx}{dt} + f(x, \lambda) = 0. \tag{27}$$

At the $1:4$ SS/H point, one obtains the following normal form equations. Let $z = (z_0, z_1, z_2) \in \mathbb{C}^3$, where z_0 is the coordinate of the steady-state mode and (z_1, z_2) are the coordinates of the Hopf mode. The normal form equations to quintic order, with only a minimal set of relevant terms, are given by:

$$\phi(z, \lambda, a, \tau) = \begin{pmatrix} p^1 z_0 + i(|z_1|^2 - |z_2|^2)p^2 z_0 \\ (q^1 + a + q^3|z_2|^2)z_1 - i(q^2 + |z_2|^2 q^4 - (1+\tau))z_1 \\ (q^1 + a + q^3|z_1|^2)z_2 - i(q^2 + |z_1|^2 q^4 - (1+\tau))z_2 \end{pmatrix}, \tag{28}$$

Parameters p^j and q^l, $j = 1, 2$, $l = 1, 2, 3$ follow the notation in Hill and Stewart [25]. These parameters are defined in terms of the coefficients of model (1). Parameter a is an unfolding parameter for the Hopf mode and, in our case, is a function of q_a, q_r. Parameter τ is associated with the phase of the Hopf mode, and we ignore it since our focus is only on the amplitudes. Denoting by λ the unfolding parameter for the steady-state mode (also a function of q_a, q_r), and by $N_0 = |z_0|^2$ and $N_1 = |z_1|^2 + |z_2|^2$, we can write

$$\begin{aligned} p^1 &= p^1(0) + p^1_\lambda(0)\lambda + p^1_{N_0}(0)N_0 + p^1_{N_1}(0)N_1 + \tfrac{1}{2}p^1_{N_0^2}(0)N_0^2 + \tfrac{1}{2}p^1_{N_1^2}(0)N_1^2, \quad p^2 = p^2(0), \\ q^1 &= q^1(0) + q^1_\lambda(0)\lambda + q^1_{N_0}(0)N_0 + q^1_{N_1}(0)N_1 + \tfrac{1}{2}q^1_{N_1^2}N_1^2, \quad q^3 = q^3(0). \end{aligned}$$

The functions q^2 and q^4 are similar to q^1 and q^3, respectively. The linear terms at the origin are

$$\begin{pmatrix} (p^1(0) + p^1_\lambda(0)\lambda)z_0 \\ (q^1(0) + a + q^1_\lambda(0)\lambda + i(q^2(0) + q^2_\lambda\lambda - (1+\tau)))z_1 \\ (q^1(0) + a + q^1_\lambda(0)\lambda + i(q^2(0) + q^2_\lambda\lambda - (1+\tau)))z_2 \end{pmatrix}.$$

At $\lambda = a = 0$, the SS/H point forces $p^1(0) = q^1(0) = 0$ and $q^2(0) \neq 0$. The real part of the eigenvalues at the origin are $p^1_\lambda(0)\lambda$ and $q^1_\lambda(0)\lambda + a$. If we assume that an asymptotically stable origin implies $\lambda < 0$, then $p^1_\lambda(0) < 0$.

5.1.1 Weakly-nonlinear analysis

In the following, we perform a weakly nonlinear analysis of the spatially homogeneous steady states $(u^+, u^-)=(u^*, u^*)$, to obtain amplitude equations similar to the normal form equations (28). To this end, we consider perturbations of the unfolding parameters q_a and q_r, which, at the SS/H bifurcation point have the critical values $q^*_{r,a}$:

$$q_a = q_a^* + \epsilon^2 \nu_a, \quad q_r = q_r^* + \epsilon^2 \nu_r, \quad \nu_{r,a} = \pm 1, \quad 0 < \epsilon \ll 1. \tag{29}$$

We then substitute these expressions into the dispersion relation (19):

$$\sigma(k_n; q_a, q_r) = \sigma(k_n; q_a^*, q_r^*) + \frac{\partial \sigma}{\partial q_a}\epsilon^2 \nu_a + \frac{\partial \sigma}{\partial q_r}\epsilon^2 \nu_r.$$

Then, solution $u^{\pm}(x,t) \propto e^{ik_n x + i\sigma t}$ evolves on two different time scales: a fast time scale (t) and a slow time scale ($T = \epsilon^2 t$), which, in the limit $\epsilon \to 0$ can be treated as being independent [37]. Expanding $u^{\pm}$ in powers of ϵ,

$$u^{\pm}(x,t,\epsilon,T) = u^* + \epsilon u_1^{\pm} + \epsilon^2 u_2^{\pm} + \epsilon^3 u_3^{\pm} + \epsilon^4 u_4^{\pm} + \epsilon^5 u_5^{\pm} + O(\epsilon^6), \tag{30}$$

and substituting it back into the nonlinear system (1)-(3) we obtain the following abstract representation of the system:

$$0 = \mathcal{N}\left(\sum_{j\geq 1} \epsilon^j \mathbf{u_j}\right) \approx \sum_{j\geq 1} \left(\mathcal{L}(\mathbf{u_j}) - N_j - E_j\right).$$

Here, $\mathbf{u_j} = (u_j^+, u_j^-)$, $\mathcal{L}$ is the linear operator defined in Section 3.1, N_j is the nonlinear operator at $O(\epsilon^j)$ that contains the terms $u_{j-1}^{\pm}$, $u_{j-2}^{\pm}$,..., and E_j is the nonlinear operator that contains the slow-time derivatives ($\partial u_j^{\pm}/\partial T$) and the terms multiplied by ν_a, ν_r. At each $O(\epsilon^j)$ we identify the coefficients of the solutions $u_j^{\pm}$.

At $O(\epsilon^1)$, the solution is of the form

$$\begin{pmatrix} u_1^+ \\ u_1^- \end{pmatrix} = \alpha_1(T) \begin{pmatrix} v_{11} \\ v_{12} \end{pmatrix} e^{ik_1 x} + \beta_1(T) \begin{pmatrix} w_{11} \\ w_{12} \end{pmatrix} e^{ik_4 x + i\sigma_4 t} + \beta_2(T) \begin{pmatrix} w_{21} \\ w_{22} \end{pmatrix} e^{ik_4 x - i\sigma_4 t} + \text{c.c.} \tag{31}$$

Here k_1 is the steady-state wavenumber, k_4 is the Hopf wavenumber, $\sigma_4 = \sigma(k_4) \approx 0.2932$ and "c.c" stands for complex conjugate. The coefficients that appear in the solution are

$$v_{11} = v_{12} = 1, \quad w_{11} = w_{22} = k_4\gamma - \sigma_4, \quad w_{12} = w_{21} = \gamma k_4 + \sigma_4. \tag{32}$$

With this notation, we can write $w_1 = (w_{11}, w_{12})^\top = (k_4\gamma f_1 - \sigma_4 f_2)$ and $w_2 = (w_{21}, w_{22})^\top = (k_4\gamma f_1 + \sigma_4 f_2)$.

Next, we focus on the solution at $O(\epsilon^2)$. The nonlinear equation $\mathcal{L}(u_2^+, u_2^-)^\top = N_2 + E_2$ has a nontrivial solution iff $N_2 + E_2$ satisfies the Fredholm alternative, i.e., $N_2 + E_2$ is orthogonal

to the bounded solution $\hat{\mathbf{u}}$ of the adjoint homogeneous problem $\mathcal{L}^*(\hat{\mathbf{u}}) = 0$. The adjoint of the linear operator $\mathcal{L}$ is

$$\mathcal{L}^* = \begin{pmatrix} -\partial_t - \gamma\partial_x + L_1 - R_2K^+* & -L_1 + R_2K^+* \\ -L_1 + R_2K^-* & -\partial_t + \gamma\partial_x + L_1 - R_2K^-* \end{pmatrix}. \tag{33}$$

Here,

$$\hat{\mathbf{u}} = \alpha_1^a \mathbf{v}^* e^{ik_1x} + \beta_1^a \mathbf{w_1^*} e^{i\sigma_4 t + ik_4x} + \beta_2^a \mathbf{w_2^*} e^{i\sigma_4 t - ik_4x} + c.c. \tag{34}$$

The coefficients $\mathbf{v}^* = (v_1^*, v_2^*)$, $\mathbf{w}_1^* = (w_{11}^*, w_{12}^*)$ and $\mathbf{w}_2^* = (w_{21}^*, w_{22}^*)$ of the adjoint solution are given by

$$v_1^* = 1, v_2^* = \frac{i\gamma k_1 - L_1 + R_2\hat{K}^+(k_1)}{-L_1 + R_2\hat{K}^+(k_1)}, \tag{35}$$

$$w_{11}^* = w_{21}^* = 1, \quad w_{12}^* = \frac{\sigma_4 + \gamma k_4 + R_2\mathrm{Im}(\hat{K}^+(k_4))}{R_2\mathrm{Im}(\hat{K}^+(k_4))}, \quad w_{22}^* = \frac{1}{w_{12}^*}. \tag{36}$$

Here, we used the fact that at the Hopf bifurcation, $L_1 = R_2\mathrm{Re}(\hat{K}^+(k_4))$, while at the steady-state bifurcation $\gamma i k_1 = -R_2(\hat{K}^+(k_1) - \hat{K}^-(k_1))$.

Simple calculations show that $N_2 + E_2$ satisfies the Fredholm alternative, that is $\langle \hat{\mathbf{u}}, N_2 + E_2\rangle = 0$, where the inner product is defined on a Hilbert space Y

$$Y = \left\{ \mathbf{u}(x,\tau) | (x,\tau) \in [0, L_0] \times [0, \infty), \text{ s.t. } \lim_{T\to\infty} \frac{1}{T} \int_0^T \int_0^{L_0} |u| dx d\tau < \infty \right\}. \tag{37}$$

The $\mathbf{O}(2)$-invariant inner product of two vectors $\hat{\mathbf{u}} = (\hat{u}^+, \hat{u}^-)^\top$ and $\mathbf{w} = (w^+, w^-)^\top$ in Y is

$$\langle \hat{\mathbf{u}}, \mathbf{w}\rangle = \lim_{T\to\infty} \frac{1}{T} \int_0^T \int_0^{L_0 = \frac{2n\pi}{k_n}} (\hat{u}^+ \overline{w}^+ + \hat{u}^- \overline{w}^-) dx d\tau. \tag{38}$$

At $O(\epsilon^3)$, the requirement that $N_3 + E_3$ satisfies the Fredholm alternative leads to a system of differential equations for the amplitudes $(\alpha_1, \beta_1, \beta_2)$:

$$\frac{d\alpha_1}{dT} = g_1(\alpha_1, \beta_1, \beta_2, q_a, q_r), \quad \frac{d\beta_1}{dT} = g_2(\alpha_1, \beta_1, \beta_2, q_a, q_r), \quad \frac{d\beta_2}{dT} = g_3(\alpha_1, \beta_1, \beta_2, q_a, q_r). \tag{39}$$

A detailed description of these equations (and how we obtain them) can be found in the Appendix. We now have the following result.

Theorem 5.1 *The amplitude equations (39) truncated to third order obtained via the weakly-nonlinear analysis at the SS/H bifurcation point* $(q_a^0, q_r^0) \approx (1.5686, 2.7178)$ *are* $\mathbf{O(2)}$*-equivariant. The third order truncation of the right-hand side of (39) is given by the negative of the third order truncation of* (28)*. For the parameter values used in this article (which can be found in*

the caption of Figure 7), the coefficient values of these third-order truncations of the amplitude equations are

$$\begin{aligned} &p_1(0) = 0, \quad p^1_\lambda(0) = -1, \quad p^1_{N_0}(0) \approx 0.38069, \quad p^1_{N_1}(0) \approx -0.09648, \quad p^2(0) \approx 0.01293, \\ &q_1(0) = 0, \quad q^1_\lambda(0) \approx 2.63485, \quad q^1_{N_0}(0) \approx 0.95759, \quad q^1_{N_1}(0) \approx 0.03805, \quad q^3(0) \approx 0.17690, \\ &q^2_{N_0}(0) \approx -0.26016, \quad q^2_{N_1}(0) \approx 0.05666, \quad q^4(0) \approx -0.04353. \end{aligned} \tag{40}$$

The parameter values λ and a, as functions of $Q_a = q_a - q_a^*$ and $Q_r = q_r - q_r^*$, are

$$\lambda \approx 0.01858\, Q_a - 0.00496\, Q_r \quad a \approx 0.06435\, Q_r.$$

The proof of this theorem is done in the Appendix. Figure 11 shows the relationship between the q_a, q_r axes and the λ, a axes in a neighborhood of the SS/H point.

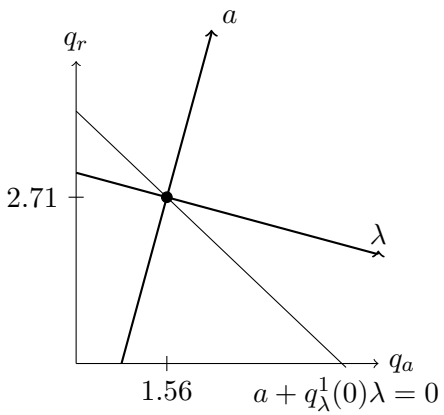

Figure 11: Relationship between the q_a, q_r axes and λ, a axes. The a axis is the steady-state bifurcation curve while $a + q^1_\lambda(0)\lambda = 0$ is the Hopf line.

5.1.2 Existence and stability of solution branches

The nondegeneracy conditions for the unfolding of the SS/H point with $\mathbf{O(2)}$ symmetry, using only leading order terms, are derived in [25] and given in Table 5 along with their signs obtained from Theorem 5.1.

Primary branches Using the third order truncation we can determine the branching and stability of the primary bifurcating branches: stationary pulse, rotating wave and standing wave. Recall the notation from Section 4.2. The branching equations are given in Table 6 where $(\cdot)$ are the labels for the expressions in Table 5. For fixed values of a, the stationary pulse bifurcates supercritically as λ increases across the steady-state bifurcation curve (a-axis). For small a values, the standing waves and rotating waves bifurcate subcritically as λ increases

No	condition	sign	No	condition	sign
(1)	$p^1_{N_0}(0)$	(+)	(6)	$2q^1_{N_0}(0)p^1_{N_1}(0) - (2q^1_{N_1}(0) + q^3(0))p^1_{N_0}(0)$	(−)
(2)	$p^1_\lambda(0)$	(−)	(7)	$q^1_{N_0}(0)p^1_\lambda(0) - q^1_\lambda(0)p^1_{N_0}(0)$	(−)
(3)	$q^1_{N_1}(0)$	(+)	(8)	$2p^1_{N_1}(0)q^1_\lambda(0) - (2q^1_{N_1}(0) + q^3)p^1_\lambda(0)$	(−)
(4)	$q^1_\lambda(0)$	(+)	(9)	q^3	(+)
(5)	$2q^1_{N_1}(0) + q^3(0)$	(+)	(10)	$q^1_{N_1}(0) + q^3$	(+)

Table 5: Nondegeneracy conditions for unfolding the Steady-State/Hopf bifurcation with $\mathbf{O(2)}$ symmetry using only leading order terms.

across the Hopf curve. We now look at the sign of the eigenvalues at the bifurcation point, the expressions are taken from [25]. Recall that because the normal form comes from (27), positive

Solution	Isotropy Subgroup	Branching equation	Stability property
SP	$\mathbb{Z}_2(\kappa) \times \mathbf{S}^1$	$\lambda = -(1)N_0/(2)$	stable
RW	$\widetilde{\mathbf{SO}}(2)$	$(4)\lambda = -(a + (3)N_1)$	unstable
SW	$\mathbb{Z}_2(\kappa) \times Z^{(\pi/4,\pi)}$	$(4)\lambda = -(a + (5)N_1)$	unstable

Table 6: Isotropy subgroup, branching equation and stability of primary bifurcating solutions: SP, RW, SW.

real parts correspond to stable directions and negative real parts to unstable directions. For the stationary pulse, the real parts of the eigenvalues are 0, $p^1_{N_0}(0) > 0$ and q^1 evaluated at $(x_0, 0, 0)$; that is,

$$(q^1_\lambda(0)p^1_{N_0} + q^1_{N_0}(0))x_0^2 \approx 1.94x_0^2 > 0.$$

Therefore, the SP branch is asymptotically stable.

For the rotating wave, the eigenvalues are 0, $q^1_{N_1}(0) > 0$ and two other complex eigenvalues with real parts, q^3 and p^1 evaluated at $(0, x_1, 0)$. We know $q^3(0) > 0$ and so $q^3 > 0$ for (λ, a) in a small neighborhood of $(0, 0)$. Now, for a fixed a, substituting λ with the branching equation (see Table 6) we obtain

$$p^1 = \frac{a}{(4)} + \left(\frac{(3)}{(4)} + p^1_{N_1}(0)\right) N_1 \approx \frac{a}{(4)} - 0.081N_1.$$

Thus, $p^1 < 0$ for $a < 0$ and $p^1 > 0$ for $a > 0$ and for N_1 small. Therefore, for $a < 0$, the RW branch has two eigenvalues with positive real part at bifurcation and one eigenvalue with negative real part. Moreover, the RW branch is asymptotically stable for $a > 0$. Note that

for $a > 0$, a Hopf bifurcation occurs as p^1 changes sign for N_1 large enough, and at this point a MRW bifurcates from RW. We do not investigate the stability of this bifurcating solution. However, the numerical simulations suggest that it is asymptotically stable for a large range of parameter values.

For the standing wave branch, the real parts of the eigenvalues are 0, p^1, $2q^1_{N_1}(0)+q^3(0)$ and $-q^3(0)x_1^2$, which are evaluated at $(0, x_1, x_1)$. We know that $2q^1_{N_1}(0)+q^3(0) > 0$ and $-q^3(0) < 0$ (see Table 5). Thus, the SW branch is unstable. Note that,

$$p^1 = \frac{a}{(4)} + \left(\frac{(5)}{(4)} + p^1_{N_1}(0)\right) N_1 \approx \frac{a}{(4)} - 0.01N_1.$$

This means $p^1 < 0$ for $a < 0$ and $p^1 > 0$ for $a > 0$ small enough.

Secondary bifurcations: fifth-order truncation We now investigate the appearance of secondary branches of periodic solutions bifurcating from the primary branches. To this end, we consider the fifth-order truncation of (28). We only need to study a few cases involving $p^1_{N_1^2}(0)$ and $q^1_{N_1^2}(0)$ which, along with the numerical simulations, enables us to make educated guesses on possible bifurcation diagrams. Submaximal periodic solutions with isotropy subgroups $\mathbb{Z}_2(\kappa)$ and $\mathbb{Z}_2(\kappa L/8, \pi/\sigma_4)$ have both orbit representative (x_0, x_1, x_1). In this case we must solve

$$\begin{aligned} &p^1_\lambda(0)\lambda + p^1_{N_0}(0)x_0^2 + 2p^1_{N_1}(0)x_1^2 + 2p^1_{N_1^2}(0)x_1^4 = 0,\\ &a + q^1_\lambda(0)\lambda + q^1_{N_0}(0)x_0^2 + 2q^1_{N_1}(0)x_1^2 + 2q^1_{N_1^2}(0)x_1^4 + q^3x_1^2 = 0. \end{aligned}$$

This is done by solving the first equation for x_0^2, and then substituting it into the second equation. The second equation is then solved for λ. After substituting λ in the first equation one obtains (in the notation of [25])

$$\lambda = \frac{(1)a}{(7)} - \frac{(6)}{(7)}x_1^2 + \frac{2c_1}{(7)}x_1^4, \qquad a(2) = (8)x_1^2 - (7)x_0^2 - 2c_2x_1^4, \tag{41}$$

where

$$c_1 = q^1_{N_1^2}(0)p^1_{N_0}(0) - q^1_{N_0}(0)p^1_{N_1^2}(0) \quad \text{and} \quad c_2 = 2q^1_{N_1^2}(0)p^1_\lambda(0) - p^1_{N_1^2}(0)q^1_\lambda(0).$$

The first equation can always be satisfied because λ is unconstrained. By fixing parameter a, the existence of a bifurcating branch only depends on solving the second equation in (41); that is,

$$x_1^2 = \frac{(8)}{4c_2} \pm \frac{1}{4c_2}\sqrt{(8)^2 + 8c_2(a - (7)x_0^2)}. \tag{42}$$

We now investigate the existence of secondary branches of periodic solutions bifurcating from SP and SW. For $x_0 = 0$ and $N_1 > 0$ the secondary branch connects to SW, while for $x_1 = 0$ and $N_0 > 0$ the secondary branch connects to SP. In particular, we show that a secondary branch of solutions can connect the SP and SW branches. Recall that $(7), (8) < 0$.

(1) If $c_2 < 0$, both solutions in (42) exist. In the case $a > 0$, notice that the right-hand side of (42) is positive for both "+" and "−" solutions. For $x_0 = 0$, we have two x_1^2 solutions. If $x_1 = 0$, there are no solutions in x_0. Therefore, the secondary branch connects to SW at two different locations. If $a < 0$, then $x_1 = 0$ for $x_0^2 = a/(7)$ in the "+" solution. In the "−" solution, setting $x_0 = 0$ yields a positive right-hand side. The "+" and "−" branches meet at the x_0 value that makes the square root vanish. Thus, the secondary branch connects the SP and SW primary branches.

(2) If $c_2 > 0$, the "−" solution is negative and the "+" solution is non-negative if and only if $a - (7)x_0^2 > 0$. We see that $x_1 = 0$ if and only if $a - (7)x_0^2 = 0$ which only occurs for $a < 0$. Thus, the secondary branch connects to the SP branch. If $x_0 = 0$, then the right-hand side of the "+" solution is positive if $a > 0$, and so the secondary branch connects to SW.

Figure 12 shows the bifurcation diagrams obtained for the parameter values discussed in Theorem 5.1 for $p^1_{N_1^2}(0) = 0$ and $q^1_{N_1^2}(0) = \pm 0.01$. Note that in these diagrams, $X = x_0 + x_1$.

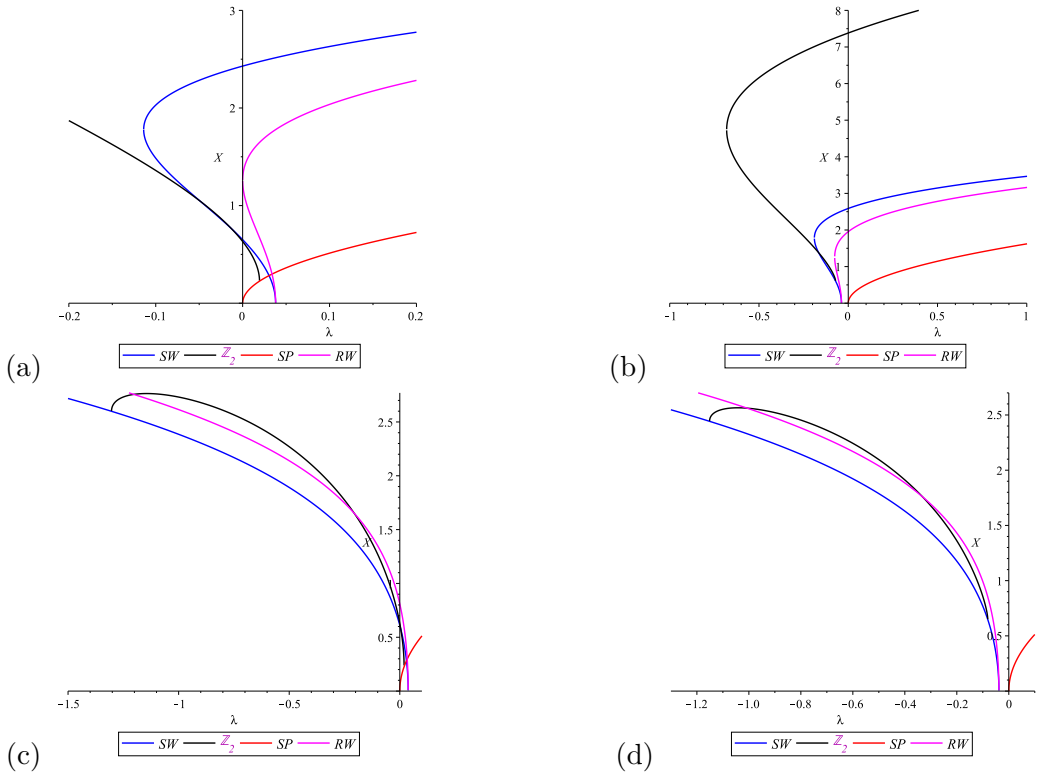

Figure 12: Bifurcation diagrams associated with the two cases $c_2 > 0$ and $c_2 < 0$: (a) $c_2 > 0$, $a < 0$; (b) $c_2 > 0$, $a > 0$; (c) $c_2 < 0$, $a < 0$; (d) $c_2 < 0$, $a > 0$.

We now use the rigorous analytical results that gave us the primary branches, combined with the numerical simulations, to select a possible bifurcation diagram from the two scenarios for secondary bifurcations ($c_2 > 0$, $c_2 < 0$). Numerical simulations of Figure 7 (d) and (g)

each show a $\mathbb{Z}_2(\kappa)$ periodic solutions near the steady-state bifurcation line, but with fine details of the pattern close to SP and SW respectively. This suggests a secondary branch of $\mathbb{Z}_2(\kappa)$ periodic solutions connecting the SP and SW branches. This is the situation seen for $c_2 < 0$ and we conjecture that this is the situation happening in this case. In Figure 13 we produce a rough gyratory bifurcation diagram illustrating the $c_2 < 0$ situation. In addition, we know that a MRW bifurcates from RW for $a > 0$ if N_1 is large enough, we added a plausible branch given that the MRW is observed to be asymptotically stable in the numerical simulations. We name the periodic solution with isotropy subgroup $\mathbb{Z}_2(\kappa)$ *modulated standing pulse* (MSP) and the periodic solution with isotropy subgroup $\mathbb{Z}_2(\kappa L/8, \pi/\omega)$ *modulated standing wave* (MSW). The location of those branches is conjectural.

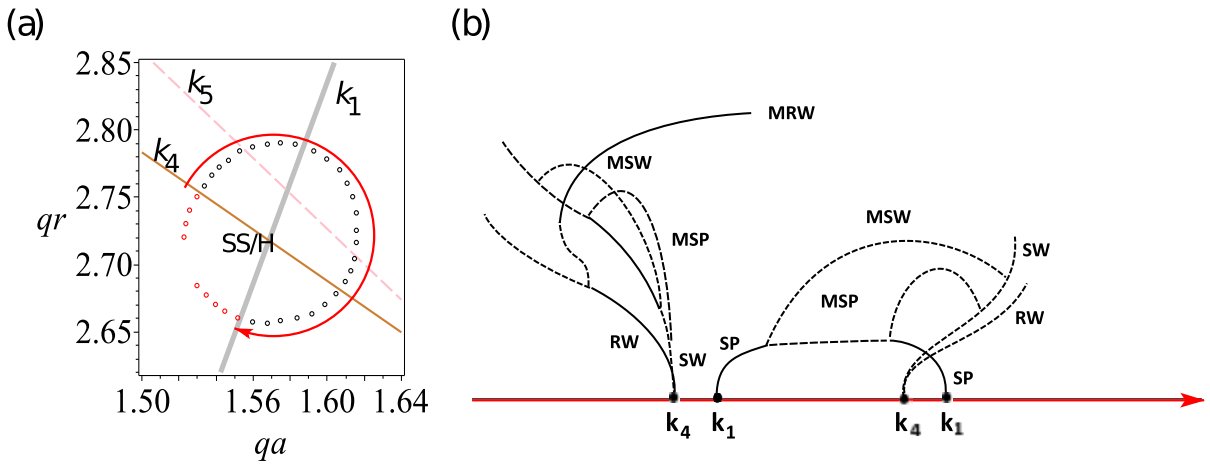

Figure 13: (a) Path around the SS/H point. (b) Potential circular bifurcation diagram corresponding, from left to right, to the clockwise direction on the path around the SS/H point. The bifurcation diagram is based on $c_2 < 0$ in Figure 12. The left-hand part correponds to $a > 0$ and the right-hand part for $a > 0$ (but reflected about the X axis). The location of the MRW branch is conjectural, but based on numerical simulations. SP: stationary pulse, SW: standing wave, RW: rotating wave, MS(P/W): modulated standing pulse/wave.

6 Discussion

In this article, we investigated the bifurcation dynamics of a large variety of complex spatial and spatio-temporal patterns exhibited by a nonlocal hyperbolic model for self-organised animal aggregation. It is shown in [15] that simple, classical patterns such as stationary waves (pulses) and travelling trains are the result of codimension-1 subcritical Hopf and steady-state bifurcations. Here, we focused on the more complex patterns that arise near codimension-two bifurcation points, and used symmetry and bifurcation theory to provide a rigorous classification of these patterns.

6.1 Biological implications

Many of the patterns identified analytically and numerically in the vicinity of codimension-two bifurcations are unstable (as shown by the sign of the coefficients of the amplitude equations) and usually undergo a cascade of other bifurcations to heterogenous patterns or to stable spatially homogeneous steady states (as observed numerically; see Figures 7,10 and 13). This raises the question of whether all transitions between group patterns observed in nature (e.g., from moving to stationary aggregations) are actually generated by changes in the needs of individuals (which are modelled mathematically by changes in parameter values; see [10] for a discussion on group patterns obtained for different parameter values in a model for self-organised aggregations). Our results here suggest that it could be possible that some behavioural transitions observed in nature are actually intrinsic to group dynamics, thus occurring for the same parameter values.

In regard to the stability of solutions (patterns), we also remark that the most common patterns (e.g., stationary pulses describing resting animals, or rotating waves describing travelling/migrating aggregations) are usually stable, and can be observed for longer periods of time (as shown in Figures 7 and 10). In contrast, the most complex patterns (e.g., standing waves and modulated standing waves) are usually transient, as shown numerically and analytically in Figures 7 and 13(b). This raises the question of whether animal aggregations might also exhibit some complex spatial and spatio-temporal patterns, which are more difficult to identify experimentally or through observations because of the very short display time.

6.2 Mathematical observations

A rigorous study of the local bifurcation dynamics for equation (1) requires the use of reduction methods to investigate the bifurcation equations. This was done in [15] (using weakly nonlinear analysis) for the steady-state and the Hopf bifurcations in model M2. In particular, it was shown that stationary pulses and travelling waves bifurcate subcritically. More recently, weakly nonlinear analysis was used to investigate the $\mathbf{O}(\mathbf{2})$ Hopf/Hopf mode interaction in model M4 [7], and partial results about the existence and stability of bifurcating solutions were computed. In particular, it was shown that the Rotating Waves (RW) and Standing Waves (SW) are subcritical (and so unstable) near the bifurcation. In this study we also used weakly nonlinear analysis to obtain the coefficients of the cubic-order truncation of the amplitude equations. These findings reinforce the idea that observable patterns of (relatively) large amplitude occur as threshold conditions via hard loss of stability from a subcritical bifurcation, rather than from incremental steps which arise from supercritical bifurcations.

In order to perform a centre manifold reduction or a Lyapunov-Schmidt reduction on model (1), we need to check that those methods can be applied for this system of partial differential equations. For certain classes of first-order semilinear hyperbolic equations (seen for instance in laser dynamics [35, 30]), spectral results have been obtained, which guarantee the application of the centre manifold reduction [35]. Also, results about the Fredholmness of the linear operator have been obtained in order to perform Lyapunov-Schmidt reductions [30]. However, because of the nonlocal nature of the turning functions, equation (1) does not fall into the category studied in these papers. In consequence, new results concerning the use of reduction methods for first-order

hyperbolic equations with nonlocal terms are the subject of future work.

Although the local study of codimension-two bifurcations can yield some results of more global nature, many of the patterns observed in numerical simulations occur far from equilibrium. In particular, we would be interested in continuing the bifurcated solutions (whether stable or unstable) and observe the symmetry-breaking process, as we vary certain parameters. A numerical continuation software for equation (1) is being developed by Kovacic [31]. This software will permit to trace the emergence of some of the more exotic symmetry-broken patterns such as traveling breathers and feathers [13], and also possibly the existence of asymptotically stable robust heteroclinic cycles.

Acknowledgments

PLB would like to thank Mitchell Kovacic and Lennaert van Veen for useful discussions. PLB and RE would like to thank Marty Golubitsky and Mark A. Lewis for fruitful discussions at the early stages of this project. PLB acknowledges the funding support from NSERC (Canada) in the form of a Discovery Grant. RE acknowledges support from a NRP Scotland Early Career Researcher Exchange Award and an EPSRC First Grant.

A Appendix

In the following, we focus on the SS/H case and show the details of the weakly nonlinear analysis of the spatially homogeneous steady states $(u^+,u^-)=(u^*,u^*)$. (The aim of this analysis is to obtain amplitude equations similar to the normal form equations (28)).

Recall that at $O(\epsilon^1)$, the solution is of the form

$$\begin{pmatrix} u_1^+ \\ u_1^- \end{pmatrix} = \alpha_1(T)\begin{pmatrix} v_{11} \\ v_{12} \end{pmatrix} e^{ik_1x} + \beta_1(T)\begin{pmatrix} w_{11} \\ w_{12} \end{pmatrix} e^{ik_4x+i\sigma_4t} + \beta_2(T)\begin{pmatrix} w_{21} \\ w_{22} \end{pmatrix} e^{ik_4x-i\sigma_4t} + \text{c.c.} \tag{A.43}$$

At $O(\epsilon^2)$, the nonlinear terms are $N_2 = (N_2^1, -N_2^1)^T$ and $E_2 = 0$, where $N_2^1 = R_1(\hat{K}^- * u_1^+)u_1 - R_1(\hat{K}^+ * u_1^-)u_1$, with $u_1 = u_1^+ + u_1^-$. To keep the length of the exposition as short as possible, recall that $\hat{K}^\pm(k) = K^\pm * e^{ikx}$, which means $\hat{K}^+(k) = \overline{\hat{K}^-(k)}$ and $\hat{K}^\pm(k) = \hat{K}^\mp(-k)$. Define $D(k) := \hat{K}^+(k) - \hat{K}^-(k)$, $F(k) := \hat{K}^+(k) + \hat{K}^-(k)$, which means $D(k) \in i\mathbb{R}$ and $F(k) \in \mathbb{R}$. Finally, let $H_1(k) = k_4\gamma D(k) + \sigma_4 F(k)$. Therefore,

$$\begin{aligned} N_2^1 \;=\; & \mathcal{E}_{(0,2k_1)}\alpha_1^2 e^{2ik_1x} + \mathcal{E}_{(\sigma_4,k_1+k_4)}\alpha_1\beta_1 e^{i((k_1+k_4)x+\sigma_4t)} + \mathcal{E}_{(\sigma_4,k_1-k_4)}\alpha_1\beta_2 e^{i((k_1-k_4)x+\sigma_4t)} \\ & + \mathcal{E}_{(-\sigma_4,k_1-k_4)}\alpha_1\overline{\beta}_1 e^{i((k_1-k_4)x-\sigma_4t)} + \mathcal{E}_{(-\sigma_4,k_1+k_4)}\alpha_1\overline{\beta}_2 e^{i((k_1+k_4)x-\sigma_4t)} + \mathcal{E}_{(2\sigma_4,2k_4)}\beta_1^2 e^{2ik_4x+2i\sigma_4t} \\ & + \mathcal{E}_{(2\sigma_4,-2k_4)}\beta_2^2 e^{-2ik_4x+2i\sigma_4t} + \mathcal{E}_{(0,2k_4)}\beta_1\overline{\beta}_2 + \mathcal{E}_{(0,0)}(|\beta_1|^2 - |\beta_2|^2) + \text{c.c.} \end{aligned}$$

with

$$\begin{aligned}
&\mathcal{E}_{(0,2k_1)} = -2D(k_1)R_1, && \mathcal{E}_{(\sigma_4,k_1+k_4)} = -2R_1(k_4\gamma D(k_1) + H_1(k_4)),\\
&\mathcal{E}_{(\sigma_4,k_1-k_4)} = -2R_1(k_4\gamma D(k_1) - H_1(k_4)), && \mathcal{E}_{(-\sigma_4,k_1-k_4)} = -2R_1(k_4\gamma D(k_1) + \overline{H}_1(k_4)),\\
&\mathcal{E}_{(-\sigma_4,k_1+k_4)} = -2R_1(k_4\gamma D(k_1) - \overline{H}_1(k_4)), && \mathcal{E}_{(2\sigma_4,2k_4)} = -2k_4\gamma R_1 H_1(k_4),\\
&\mathcal{E}_{(2\sigma_4,-2k_4)} = 2R_1k_4\gamma H_1(k_4), && \mathcal{E}_{(0,2k_4)} = -4(k_4\gamma)^2 D(k_4)R_1,\\
&\mathcal{E}_{(0,0)} = 2k_4\gamma\sigma_4 F(k_4)R_1,
\end{aligned}$$

where for $(a,b) \neq (0,0)$, $\mathcal{E}_{(a,-b)} = -\mathcal{E}_{(a,b)}$. Note also that $\mathcal{E}_{(-a,-b)} = \overline{\mathcal{E}}_{(a,b)}$.

Simple calculations show that $N_2 + E_2$ satisfies the Fredholm alternative, that is $\langle \hat{\mathbf{u}}, N_2 + E_2\rangle = 0$, with $\hat{\mathbf{u}}$ the solution of the adjoint homogeneous problem $\mathcal{L}^*(\hat{\mathbf{u}}) = 0$. Thus, equation $\mathcal{L}(\mathbf{u_2}) = N_2 + E_2$ has a nontrivial solution given by

$$\begin{aligned}
\begin{pmatrix} u_2^+ \\ u_2^- \end{pmatrix} \;=\; & \alpha_3(T)\mathbf{v_3}e^{ik_1x}f_1 + \beta_3(T)\mathbf{w_3}e^{i\sigma_4t+ik_4x} + \beta_4(T)\mathbf{w_4}e^{i\sigma_4t-ik_4x} + \mathcal{G}_{(0,2k_1)}\alpha_1^2e^{2ik_1x}\\
&+\mathcal{G}_{(\sigma_4,k_1+k_4)}\alpha_1\beta_1e^{i((k_1+k_4)x+\sigma_4t)} + \mathcal{G}_{(\sigma_4,k_1-k_4)}\alpha_1\beta_2e^{i((k_1-k_4)x+\sigma_4t)}\\
&+\mathcal{G}_{(-\sigma_4,k_1-k_4)}\alpha_1\overline{\beta}_1e^{i(k_1-k_4)x-\sigma_4t)} + \mathcal{G}_{(-\sigma_4,k_1+k_4)}\alpha_1\overline{\beta}_2e^{i((k_1+k_4)-\sigma_4t)} \qquad \text{(A.44)}\\
&+\mathcal{G}_{(2\sigma_4,2k_4)}\beta_1^2e^{2i(k_4x+\sigma_4t)} + \mathcal{G}_{(2\sigma_4,-2k_4)}\beta_2^2e^{2i(-k_4x+\sigma_4t)} + \mathcal{G}_{(0,2k_4)}\beta_1\overline{\beta}_2e^{2ik_4x}\\
&+\mathcal{G}_{(0,0)}(|\beta_1|^2 - |\beta_2|^2) + \text{c.c.} \qquad \text{(A.45)}
\end{aligned}$$

with $\mathcal{G}_{(a,b)} = (\mathcal{G}^1_{(a,b)}, \mathcal{G}^2_{(a,b)})^T$. We let

$$J_{(a,b)} = ia^2 - \gamma^2b^2i + 2aL_1 - R_2\gamma bD(b) - R_2aF(b).$$

Note that $J_{(-a,b)} = -\overline{J}_{(a,b)}$ and $J_{(a,-b)} = J_{(a,b)}$. Then, for $a \neq 0$

$$\mathcal{G}^1_{(a,b)} = \frac{-(a-\gamma b)\mathcal{E}_{(a,b)}}{J_{(a,b)}}, \qquad \mathcal{G}^2_{(a,b)} = \frac{(a+\gamma b)\mathcal{E}_{(a,b)}}{J_{(a,b)}}.$$

In particular, using the symmetry properties of the indices of $\mathcal{E}_{(a,b)}$ and $J_{(a,b)}$ we have for $i = 1, 2$

$$\mathcal{G}^1_{(-a,b)} = \overline{\mathcal{G}}^2_{(a,b)}. \qquad \text{(A.46)}$$

We also define $\mathcal{G}^{12}_{(a,b)} := \mathcal{G}^1_{(a,b)} + \mathcal{G}^2_{(a,b)}$. Finally,

$$\mathcal{G}^1_{(0,b)} = \mathcal{G}^2_{(0,b)} = \frac{-\mathcal{E}_{(0,b)}}{2i\gamma b + R_2D(b)} \in \mathbb{R}, \qquad \mathcal{G}^1_{(0,0)} = -\mathcal{G}^1_{(0,0)} = \frac{-\mathcal{E}_{(0,0)}}{2L_1 - R_2F(0)} \in \mathbb{R}.$$

At $O(\epsilon^3)$, the nonlinear terms $E_3 = (E_3^1, E_3^2)^\top$ and $N_3 = (N_3^1, -N_3^1)^T$ are given by

$$
\begin{aligned}
E_3 &= \begin{pmatrix} -\frac{\partial u_1^+}{\partial T} - R_2(\hat{K}_\nu^+ * u_1^-) + R_2(\hat{K}_\nu^- * u_1^+) \\ -\frac{\partial u_1^-}{\partial T} + R_2(\hat{K}_\nu^+ * u_1^-) - R_2(\hat{K}_\nu^- * u_1^+) \end{pmatrix} \\
&= \begin{pmatrix} -\frac{\partial \alpha_1}{\partial T} v_{11} e^{ik_1 x} - \frac{\partial \beta_1}{\partial T} w_{11} e^{i\sigma_4 t + ik_4 x} - \frac{\partial \beta_2}{\partial T} w_{21} e^{i\sigma_4 t - ik_4 x} - \\ R_2\Big[\big(\hat{K}_\nu^+(k_1) v_{12} - \hat{K}_\nu^-(k_1) v_{11}\big) \alpha_1(T) e^{ik_1 x} + \\ \beta_1(T) \big(\hat{K}_\nu^+(k_4) w_{12} - \hat{K}_\nu^-(k_1) w_{11}\big) e^{i\sigma_4 t + ik_4 x} + \\ \beta_2(T) \big(\hat{K}_\nu^-(k_4) w_{22} - \hat{K}_\nu^+(k_4) w_{21}\big) e^{i\sigma_4 t - ik_4 x} \Big] + \text{c.c} \\ \\ -\frac{\partial \alpha_1}{\partial T} v_{11} e^{ik_1 x} - \frac{\partial \beta_1}{\partial T} w_{11} e^{i\sigma_4 t + ik_4 x} - \frac{\partial \beta_2}{\partial T} w_{21} e^{i\sigma_4 t - ik_4 x} + \\ R_2\Big[\big(\hat{K}_\nu^+(k_1) v_{12} - \hat{K}_\nu^-(k_1) v_{11}\big) \alpha_1(T) e^{ik_1 x} + \\ \beta_1(T) \big(\hat{K}_\nu^+(k_4) w_{12} - \hat{K}_\nu^-(k_1) w_{11}\big) e^{i\sigma_4 t + ik_4 x} + \\ \beta_2(T) \big(\hat{K}_\nu^-(k_4) w_{22} - \hat{K}_\nu^+(k_4) w_{21}\big) e^{i\sigma_4 t - ik_4 x} \Big] + \text{c.c} \end{pmatrix}
\end{aligned}
$$

and

$$
\begin{aligned}
N_3^1 &= R_1 u_2 (\hat{K}^- * u_1^+ - \hat{K}^+ * u_1^-) + R_1 u_1 (\hat{K}^- * u_2^+ - \hat{K}^+ * u_2^-) \\
&\quad + S_1 (u_1^- - u_1^+) \left(\hat{K}^+ * (u_1^-)^2 - 2 \textstyle\int_0^\infty K(s) u_1^-(x+s) u_1^+(x-s)\, ds + \hat{K}^- * (u_1^+)^2 \right) \\
&\quad + 2 T_2 (\hat{K}^+ * u_1^-)(\hat{K}^- * u_1^+)(\hat{K}^+ * u_1^- - \hat{K}^- * u_1^+).
\end{aligned}
$$

Substituting the calculated solutions (u_1^+, u_1^-) and (u_2^+, u_2^-) into $(E_3 + N_3) = (N_3^1 + E_3^1, -N_3^1 - E_3^1)^\top$ we obtain:

$$
\begin{aligned}
N_3^1 + E_3^1 &= e^{ik_1 x} \Big[-\frac{d\alpha_1}{dT} F_1^1 - \alpha_1 F_1^2 + \alpha_1 |\alpha_1|^2 F_1^3 + \alpha_1 |\beta_1|^2 F_1^4 + \alpha_1 |\beta_2|^2 F_1^5 \Big] + \\
&\quad e^{i\sigma_4 t + ik_4 x} \Big[-\frac{d\beta_1}{dT} M_1^1 - \beta_1 M_1^2 + \beta_1 |\alpha_1|^2 M_1^3 + \beta_1 |\beta_1|^2 M_1^4 + \beta_1 |\beta_2|^2 M_1^5 \Big] + \\
&\quad e^{i\sigma_4 t - ik_4 x} \Big[-\frac{d\beta_2}{dT} N_1^1 - \beta_2 N_1^2 + \beta_2 |\alpha_1|^2 N_1^3 + \beta_2 |\beta_2|^2 N_1^4 + \beta_2 |\beta_1|^2 N_1^5 \Big]. \quad \text{(A.47)}
\end{aligned}
$$

The second component of the coefficients vectors $F^j = (F_1^j, F_2^j)^\top$, $M^j = (M_1^j, M_2^j)^\top$ and $N^j = (N_1^j, N_2^j)^\top$, $j = 2, 3, 4, 5$ is given by

$$
F_2^j = -F_1^j, \quad M_2^j = -M_1^j, \quad N_2^j = -N_1^j, \quad j = 2, 3, 4, 5. \tag{A.48}
$$

Finally, we have $F_1^1 = v_{11}$, $F_2^1 = v_{12}$, $M_1^1 = w_{11}$, $M_2^1 = w_{12}$, $N_1^1 = w_{21}$ and $N_2^1 = w_{22}$. Set $w_{1p} = w_{11} + w_{12}$ and $w_{1m} = w_{11} - w_{12}$. To calculate the coefficient vectors F_1^j, M_1^j and N_1^j, $j \geq 2$, we define the following expressions which appear as parts of the coefficients of monomials in N_3^1:

$$
A_2 = 2w_{11}\hat{K}^-(k_1 + k_4) + 2w_{12}\hat{K}^+(k_1 + k_4) - 2w_{11}\hat{K}^+(k_1 - k_4) - 2w_{12}\hat{K}^-(k_1 - k_4) \in \mathbb{C} \tag{A.49}
$$

and

$$\begin{aligned}
b_2 &= -\mathcal{G}^1_{(0,0)}F(0),\\
b_6 &= -\mathcal{G}^1_{(0,2k_4)}D(2k_4),\\
b_7 &= \mathcal{G}^1_{(\sigma_4,k_1+k_4)}\hat{K}^-(k_1+k_4)-\mathcal{G}^2_{(\sigma_4,k_1+k_4)}\hat{K}^+(k_1+k_4),\\
b_8 &= \mathcal{G}^1_{(\sigma_4,k_1-k_4)}\hat{K}^-(k_1-k_4)-\mathcal{G}^2_{(\sigma_4,k_1-k_4)}\hat{K}^+(k_1-k_4),\\
b_9 &= \mathcal{G}^1_{(-\sigma_4,k_1-k_4)}\hat{K}^-(k_1-k_4)-\mathcal{G}^2_{(-\sigma_4,k_1-k_4)}\hat{K}^+(k_1-k_4),\\
b_{10} &= \mathcal{G}^1_{(-\sigma_4,k_1+k_4)}\hat{K}^-(k_1+k_4)-\mathcal{G}^2_{(-\sigma_4,k_1+k_4)}\hat{K}^+(k_1+k_4),\\
b_{11} &= \mathcal{G}^1_{(2\sigma_4,2k_4)}\hat{K}^-(2k_4)-\mathcal{G}^2_{(2\sigma_4,2k_4)}\hat{K}^+(2k_4). \qquad \text{(A.50)}
\end{aligned}$$

Coefficients of the steady-state mode in the N_3+E_3 terms:

Denote by $\mathrm{Re}(\hat{K}(\cdot))=\mathrm{Re}(\hat{K}^{\pm}(\cdot))$ and $\mathrm{Im}(\hat{K}(\cdot))=\mathrm{Im}(\hat{K}^{\pm}(\cdot))$. The coefficient of $\alpha_1(T)$ is $F^2=(F_1^2,F_2^2)^\top$, with $F_1^2=F_1^{2,r}+iF_1^{2,i}$, $F_2^2=-F_1^2$ and

$$F^{2,r} = 0, \quad F^{2,i}=R_2v_{11}D_\nu(k_1).$$

Thus $F^2\in i\mathbb{R}$. The coefficient of $\alpha_1|\alpha_1|^2$ is $F^3=(F_1^3,F_2^3)^\top$, with $F_1^3=F_1^{3,r}+iF_1^{3,i}$, $F_2^3=-F_1^3$ and

$$F_1^{3,r}=0, \quad F_1^{3,i}=-3T_2\Big[3\mathrm{Re}(\hat{K}(k_1))+3\mathrm{Re}(\hat{K}(k_1))-\mathrm{Im}(\hat{K}(3k_1))-\mathrm{Im}(\hat{K}(3k_1))\Big].$$

The coefficient of $\alpha_1|\beta_1|^2$ is $F^4=(F_1^4,F_2^4)^\top$, $F_1^4=F_1^{4,r}+iF_1^{4,i}$, $F_2^4=-F_1^4$ and

$$\begin{aligned}
F_1^{4,r} &= R_1\mathrm{Re}\Big(-H_1(k_4)\mathcal{G}^{12}_{(-\sigma_4,(k_1-k_4))}-\overline{H_1(k_4)}\mathcal{G}^{12}_{(\sigma_4,k_1+k_4)}+2b_2+w_{1p}(b_9+b_7)\Big),\\
F_1^{4,i} &= R_1\mathrm{Im}\Big(-D(k_1)\mathcal{G}^{12}_{(0,0)}-H_1(k_4)\mathcal{G}^{12}_{(-\sigma_4,k_1-k_4)}-\overline{H_1(k_4)}\mathcal{G}^{12}_{(\sigma_4,k_1+k_4)}+w_{1p}(b_9+b_7)\Big)\\
&\quad -S_1w_{1m}(A_2-\overline{A}_2)-6T_2\Big[2(w_{11}^2+w_{12}^2)\mathrm{Im}(\hat{K}(k_1))+2w_{11}w_{12}\mathrm{Im}(\hat{K}(k_1-2k_4))\\
&\quad +2w_{11}w_{12}\mathrm{Im}(\hat{K}(k_1+2k_4))\Big].
\end{aligned}$$

The coefficient of $\alpha_1|\beta_2|^2$ is $F^5=(F_1^5,F_2^5)$, with $F_1^5=F_1^{5,r}+iF_1^{5,i}$, $F_2^5=-F_1^5$ and

$$\begin{aligned}
F_1^{5,r} &= R_1\mathrm{Re}\Big(H_1(k_4)\mathcal{G}^{12}_{(-\sigma_4,k_1+k_4)}+\overline{H_1(k_4)}\mathcal{G}^{12}_{(\sigma_4,(k_1-k_4))}-2b_2+w_{1p}(b_{10}+b_8)\Big),\\
F_1^{5,i} &= R_1\mathrm{Im}\Big(-D(k_1)\mathcal{G}^{12}_{(0,0)}+H_1(k_4)\mathcal{G}^{12}_{(-\sigma_4,k_1+k_4)}+\overline{H_1(k_4)}\mathcal{G}^{12}_{(\sigma_4,k_1-k_4)}+w_{1p}(b_{10}+b_8)\Big)\\
&\quad -S_1w_{1m}(A_2-\overline{A}_2)-6T_2\Big[2(w_{11}^2+w_{12}^2)\mathrm{Im}(\hat{K}(k_1))+2w_{11}w_{12}\mathrm{Im}(\hat{K}(k_1-2k_4))\\
&\quad +2w_{11}w_{12}\mathrm{Im}(\hat{K}(k_1+2k_4))\Big].
\end{aligned}$$

Since $\mathcal{G}^{12}_{(-a,b)}=\overline{\mathcal{G}}^{12}_{(a,b)}$ and $b_8+b_{10}=-\overline{(b_7+b_9)}$, we then obtain $F_1^{4,r}=-F_1^{5,r}$ and $F_1^{4,i}=F_1^{5,i}$.

Coefficients of the Hopf mode in the $N_3 + E_3$ terms:

The coefficients of the monomials $\beta_1, \beta_1|\alpha_1|^2, \beta_1|\beta_1|^2, \beta_1|\beta_2|^2$ are denoted, respectively, by $M^j = (M_1^j, M_2^j)^T$, $j = 2,3,4,5$. The coefficients of the monomials $\beta_2, \beta_2|\alpha_1|^2, \beta_2|\beta_2|^2, \beta_2|\beta_1|^2$ are denoted, respectively, by $N^j = (N_1^j, N_2^j)^T$, $j = 2,3,4,5$. Moreover, $M_2^j = -M_1^j$ and $N_2^j = -N_1^j$ for $j = 2,3,4,5$. Finally, one can verify that $N_1^j = -M_1^j$ for $j = 3,4,5$, and so we only need to compute the terms M_1^j for $j = 2,3,4,5$. Therefore we have

$$\begin{aligned} M_1^{2,r} &= -R_2\mathrm{Re}(w_{12}\hat{K}_\nu^+(k_4) - w_{11}\hat{K}_\nu^-(k_4)), \quad M_1^{2,i} = -R_2\mathrm{Im}(w_{12}\hat{K}_\nu^+(k_4) + w_{11}\hat{K}_\nu^-(k_4)), \\ N_1^{2,r} &= -R_2\mathrm{Re}(w_{22}\hat{K}_\nu^-(k_4) - w_{21}\hat{K}_\nu^+(k_4)), \quad N_1^{2,i} = -R_2\mathrm{Im}(w_{22}\hat{K}_\nu^-(k_4) + w_{21}\hat{K}_\nu^+(k_4)), \end{aligned}$$

and

$$\begin{aligned} M_1^{3,r} &= R_1\mathrm{Re}\Big[(-D(k_1)\mathcal{G}^1_{(\sigma_4,k_4-k_1)} + D(k_1)\mathcal{G}^1_{(\sigma_4,k_1+k_4)}) + 2(\bar{b}_9 + b_7)\Big] + 12S_1\sigma_4\hat{K}(0) \\ &\quad -6(w_{11} - w_{12})T_2\Big[2\mathrm{Re}(\hat{K}(k_4)) - \mathrm{Re}(\hat{K}(k_4 + 2k_1)) - \mathrm{Re}(\hat{K}(k_4 - 2k_1))\Big], \\ M_1^{3,i} &= R_1\mathrm{Im}\Big[(-D(k_1)\mathcal{G}^1_{(\sigma_4,k_4-k_1)} + D(k_1)\mathcal{G}^1_{(\sigma_4,k_1+k_4)}) + 2(\bar{b}_9 + b_7)\Big] - \\ &\quad 6(w_{11} + w_{12})T_2\Big[2\mathrm{Im}(\hat{K}(k_4)) - \mathrm{Im}(\hat{K}(k_4 + 2k_1)) - \mathrm{Im}(\hat{K}(k_4 - 2k_1))\Big], \end{aligned}$$

$$\begin{aligned} M_1^{4,r} &= R_1\mathrm{Re}\Big[(-H_1(k_4)\mathcal{G}^1_{(0,0)} - \overline{H}_1(k_4)\mathcal{G}^1_{(2\sigma_4,2k_4)}) + 2\gamma k_4(b_2 + b_{11})\Big] - S_1 w_{1m}\big(w_{1p}^2\mathrm{Re}(\hat{K}^+(2k_4)) \\ &\quad +\hat{K}(0)(2(w_{11}^2 + w_{12}^2) + w_{11}w_{12})\big) - 3T_2\Big[\mathrm{Re}(\hat{K}(k_4))\big(w_{11}(w_{11}^2 + 2w_{12}^2) - w_{12}(2w_{11}^2 + w_{12}^2)\big) \\ &\quad -\mathrm{Re}(\hat{K}(3k_4))(w_{12}w_{11}^2 - w_{12}^2w_{11})\Big], \\ M_1^{4,i} &= R_1\mathrm{Im}\Big[(-H_1(k_4)\mathcal{G}^1_{(0,0)} - \overline{H}_1(k_4)\mathcal{G}^1_{(2\sigma_4,2k_4)}) + 2\gamma k_4(b_2 + b_{11})\Big] - S_1 w_{1p}w_{1m}^2\mathrm{Im}(\hat{K}^+(2k_4)) - \\ &\quad 3T_2\Big[\mathrm{Im}(\hat{K}(k_4))\big(w_{11}(w_{11}^2 + 2w_{12}^2) + w_{12}(2w_{11}^2 + w_{12}^2)\big) - \mathrm{Im}(\hat{K}(3k_4))\big(w_{12}w_{11}^2 + w_{12}^2w_{11}\big)\Big], \end{aligned}$$

$$\begin{aligned} M_1^{5,r} &= R_1\mathrm{Re}\Big[(H_1(k_4)\mathcal{G}^1_{(0,0)} + H_1(k_4)\mathcal{G}^1_{(0,2k_4)}) + 2\gamma k_4(-b_2 + b_6)\Big] - \\ &\quad S_1\Big[2m_2\big((w_{11}^2 + w_{12}^2)\hat{K}(0) - 2w_{11}w_{12}\mathrm{Re}(\hat{K}(2k_4))\big) + 2m_2\big(\hat{K}(0)(w_{11} - w_{12})^2 - \\ &\quad 2w_{11}w_{12}\mathrm{Re}(\hat{K}(2k_4))\big)\Big] - 3T_2\Big[\mathrm{Re}(\hat{K}(k_4))w_{11}(2w_{12}^2 + w_{11}^2) - \\ &\quad \mathrm{Re}(\hat{K}(k_4))w_{12}(2w_{11}^2 + w_{12}^2) - \mathrm{Re}(\hat{K}(3k_4))w_{11}^2w_{12} + \mathrm{Re}(\hat{K}(3k_4))w_{12}^2w_{11}\Big], \\ M_1^{5,i} &= R_1\mathrm{Im}\Big[(H_1(k_4)\mathcal{G}^1_{(0,0)} + H_1(k_4)\mathcal{G}^1_{(0,2k_4)}) + 2\gamma k_4(-b_2 + b_6)\Big] - \\ &\quad 2S_1m_2\Big[w_{12}^2\mathrm{Im}(2\hat{k}_4) - w_{11}^2\mathrm{Im}(\hat{K}(2k_4))\Big] - 3T_2\Big[\mathrm{Im}(\hat{K}(k_4))w_{11}(2w_{12}^2 + w_{11}^2) + \\ &\quad \mathrm{Im}(\hat{K}(k_4))w_{12}(2w_{11}^2 + w_{12}^2) - \mathrm{Im}(\hat{K}(3k_4))(w_{11})^2w_{12} - \mathrm{Im}(\hat{K}(3k_4))(w_{12})^2w_{11}\Big]. \end{aligned}$$

Cubic Normal Form Equations

The Fredholm alternative requires that $N_3 + E_3$ (calculated previously) is orthogonal to the solution $\hat{\mathbf{u}}$ of the adjoint homogeneous problem $\mathcal{L}^*(\hat{\mathbf{u}}) = 0$. However, some terms in $N_3 + E_3$ do not satisfy the orthogonality condition. By imposing that these terms are zero, it leads to the following (amplitude) equations:

$$\frac{d\alpha_1}{dT} = -\alpha_1 X_1 + \alpha_1|\alpha_1|^2 X_2 + \alpha_1|\beta_1|^2 X_3 + \alpha_1|\beta_2|^2 X_4, \tag{A.51a}$$

$$\frac{d\beta_1}{dT} = -\beta_1 Y_1 + \beta_1|\alpha_1|^2 Y_2 + \beta_1|\beta_1|^2 Y_3 + \beta_1|\beta_2|^2 Y_4, \tag{A.51b}$$

$$\frac{d\beta_2}{dT} = -\beta_2 Z_1 + \beta_2|\alpha_1|^2 Z_2 + \beta_2|\beta_2|^2 Z_3 + \beta_2|\beta_1|^2 Z_4, \tag{A.51c}$$

with

$$X_1 = \frac{\overline{v}_1^* F_1^2 + \overline{v}_2^* F_2^2}{\overline{v}_1^* F_1^1 + \overline{v}_2^* F_2^1},\quad X_2 = \frac{\overline{v}_1^* F_1^3 + \overline{v}_2^* F_2^3}{\overline{v}_1^* F_1^1 + \overline{v}_2^* F_2^1},\quad X_3 = \frac{\overline{v}_1^* F_1^4 + \overline{v}_2^* F_2^4}{\overline{v}_1^* F_1^1 + \overline{v}_2^* F_2^1},\quad X_4 = \frac{\overline{v}_1^* F_1^5 + \overline{v}_2^* F_2^5}{\overline{v}_1^* F_1^1 + \overline{v}_2^* F_2^1},$$

$$Y_1 = \frac{\overline{w}_{11}^* M_1^2 + \overline{w}_{12}^* M_2^2}{\overline{w}_{11}^* M_1^1 + \overline{w}_{12}^* M_2^1},\quad Y_2 = \frac{\overline{w}_{11}^* M_1^3 + \overline{w}_{12}^* M_2^3}{\overline{w}_{11}^* M_1^1 + \overline{w}_{12}^* M_2^1},\quad Y_3 = \frac{\overline{w}_{11}^* M_1^4 + \overline{w}_{12}^* M_2^4}{\overline{w}_{11}^* M_1^1 + \overline{w}_{12}^* M_2^1},\quad Y_4 = \frac{\overline{w}_{11}^* M_1^5 + \overline{w}_{12}^* M_2^5}{\overline{w}_{11}^* M_1^1 + \overline{w}_{12}^* M_2^1},$$

$$Z_1 = \frac{\overline{w}_{11}^* N_1^2 + \overline{w}_{12}^* N_2^2}{\overline{w}_{11}^* N_1^1 + \overline{w}_{12}^* N_2^1},\quad Z_2 = \frac{\overline{w}_{11}^* N_1^3 + \overline{w}_{12}^* N_2^3}{\overline{w}_{11}^* N_1^1 + \overline{w}_{12}^* N_2^1},\quad Z_3 = \frac{\overline{w}_{11}^* N_1^4 + \overline{w}_{12}^* N_2^4}{\overline{w}_{11}^* N_1^1 + \overline{w}_{12}^* N_2^1},\quad Z_4 = \frac{\overline{w}_{11}^* N_1^5 + \overline{w}_{12}^* N_2^5}{\overline{w}_{11}^* N_1^1 + \overline{w}_{12}^* N_2^1}.$$

The X_j terms: Since $F_2^j = -F_1^j$, $j = 2, 3, 4, 5$, then the X_j terms (with $j = 1, 2, 3, 4$) can be re-written as

$$X_j = \frac{F_1^{j+1}(\overline{v}_1^* - \overline{v}_2^*)}{v_{11}(\overline{v}_1^* + \overline{v}_2^*)}.$$

Recall that $v_1^* = 1$, $v_2^* = \frac{\gamma i k_1 - L_1 + R_2\hat{K}^+(k_1)}{-L_1 + R_2\hat{K}^+(k_1)}$, and thus we have

$$\overline{v}_1^* - \overline{v}_2^* = \frac{R_2(\hat{K}^+(k_1) - \hat{K}^-(k_1))}{L_1 - R_2\hat{K}^-(k_1)} \quad \text{and} \quad \overline{v}_1^* + \overline{v}_2^* = \frac{2L_1 - R_2(\hat{K}^+(k_1) + \hat{K}^-(k_1))}{L_1 - R_2\hat{K}^-(k_1)}.$$

Moreover, since $F^{4,r} = -F^{5,r}$ and $F^{4,i} = F^{5,i}$, the real and imaginary parts of $X_3 = X_3^r + iX_3^i$ and $X_4 = X_4^4 + iX_4^i$ are

$$X_3^r = \frac{F^{4,i} R_2 \mathrm{Im}(\hat{K}^+(k_1) - \hat{K}^-(k_1))}{v_{11}\Big(2L_1 - 2R_2 Re(\hat{K}^+(k_1) + \hat{K}^-(k_1))\Big)} = X_4^r,$$

$$X_3^i = -\frac{F^{4,r} R_2 \mathrm{Im}(\hat{K}^+(k_1) - \hat{K}^-(k_1))}{v_{11}\Big(2L_1 - 2R_2 Re(\hat{K}^+(k_1) + \hat{K}^-(k_1))\Big)} = -X_4^i.$$

Therefore, the real parts of X_3 and X_4 are equal, while the imaginary parts have opposite signs, as in the normal form equations.

The Y_j, Z_j terms: since $M^j = -N^j$, $M_1^j = -M_2^j$, $N_1^j = -N_2^j$, and $\overline{w}_{11}^* = \overline{w}_{12}^* = 1$, $\overline{w}_{22}^* = \frac{1}{\overline{w}_{12}^*}$, we can write (for $j = 2, 3, 4$):

$$Y_j = \frac{\overline{w}_{11}^* M_1^{j+1} + \overline{w}_{12}^* M_2^{j+1}}{\overline{w}_{11}^* M_1^1 + \overline{w}_{12}^* M_2^1} = \frac{M_1^{j+1}(1 - \overline{w}_{12}^*)}{w_{11} + w_{12}\overline{w}_{12}^*},$$
$$Z_j = \frac{\overline{w}_{21}^* N_1^{j+1} + \overline{w}_{22}^* N_2^{j+1}}{\overline{w}_{21}^* N_1^1 + \overline{w}_{22}^* N_2^1} = \frac{N_1^{j+1}(1 - \overline{w}_{22}^*)}{N_1^1 + \overline{w}_{22}^* N_2^1} = \frac{N_1^{j+1}(1 - \frac{1}{\overline{w}_{12}^*})}{w_{21} + \frac{1}{\overline{w}_{12}^*} w_{11}} = -\frac{N_1^{j+1}(1 - \overline{w}_{12}^*)}{w_{11} + \overline{w}_{12}^* w_{12}} = Y_j.$$

Thus, the coefficients of the two Hopf equations are equal.

To compare these amplitude equations with the normal form equations, let us split the coefficients into real and imaginary parts: $Y_j = Y_j^r + iY_j^i$ and $Z_j = Z_j^r + iZ_j^i$, $j = 1, 2, 3, 4$:

$$Y_j^r = M_1^{j+1,r} \frac{(\overline{w}_{11}^* - \overline{w}_{12}^*)}{(\overline{w}_{11}^* w_{11} + \overline{w}_{12}^* w_{12})}, \quad Y_j^i = M_1^{j+1,i} \frac{(\overline{w}_{11}^* - \overline{w}_{12}^*)}{(\overline{w}_{11}^* w_{11} + \overline{w}_{12}^* w_{12})},$$
$$Z_j^r = N_1^{j+1,r} \frac{(\overline{w}_{11}^* - \overline{w}_{12}^*)}{(\overline{w}_{11}^* w_{11} + \overline{w}_{12}^* w_{12})}, \quad Z_j^i = N_1^{j+1,i} \frac{(\overline{w}_{11}^* - \overline{w}_{12}^*)}{(\overline{w}_{11}^* w_{11} + \overline{w}_{12}^* w_{12})},$$

with $M_1^{j,r}$, $M_1^{j,i}$, $N_1^{j,r}$ and $N_1^{j,i}$ the real and imaginary components calculated previously. Comparing these terms with the normal form terms leads to:

$$\begin{aligned}
&X_1^r = -(p_\lambda^1(0)\lambda), \quad X_2^r = p_{N_0}^1(0), \quad X_3^r = p_{N_1}^1(0) = X_4^r, \quad X_3^i = p^2 = -X_4^i,\\
&Y_1^r = -(a + q_\lambda^1(0)\lambda), \quad Y_2^r = q_{N_0}^1(0), \quad Y_3^r = q_{N_1}^1(0), \quad Y_4^r - Y_3^r = q^3(0),\\
&Y_1^i = -(q^2(0) + q_\lambda^2(0)\lambda) - (1 + \tau), \quad -Y_2^i = q_{N_0}^2(0), \quad -Y_3^i = q_{N_1}^2(0), \quad -(Y_4^i - Y_3^i) = q^4(0),\\
&Z_j^r = Y_j^r, \quad Z_j^i = Y_j^i, j = 1, 2, 3, 4.
\end{aligned} \tag{A.52}$$

Finally, set $\lambda = \mathrm{Re}(X_{1r})$ and solve Q_a as a function of λ and Q_r. Substitute in $\mathrm{Re}(Y_{1r})$ and normalize the Q_r term to a. Therefore, Theorem 5.1 holds true.

References

[1] T. Allen and I.M. Moroz. Hopf-Hopf and Hopf-Steady mode interactions with O(2) symmetry in Langmuir circulations. *Geophys. Astrophys. Fluid Dynamics*, 85:243–278, 1997.

[2] M. Ballerini, N. Cabibbo, R. Candelier, A. Cavagna, E. Cisbani, I. Giardina, V. Lecomte, A. Orlandi, G. Parisi, A Procaccini, M. Viale, and V. Zdravkovic. Interaction ruling animal collective betavior depends on topological rather than metric distance: evidence from a field study. *Proc. Natl. Acad. Sci.*, 105(5):1232–1237, 2008.

[3] M. Beekman, D. J. T. Sumpter, and F. L. W. Ratnieks. Phase transitions between disordered and ordered foraging in Pharaoh's ants. *Proc. Natl. Acad. Sci.*, 98(17):9703–9706, 2001.

[4] C.M. Breder. Equations descriptive of fish schools and other animal aggregations. *Ecology*, 35:361–370, 1954.

[5] H. Brumm. Causes and consequences of song amplitude adjustment in a territorial bird: a case study in nightingales. *Annal of the Brazilian Academy of Sciences*, 76(2):289–295, 2004.

[6] J. Buhl, D. J. T. Sumpter, I. D. Couzin, J. J. Hale, E. Despland, E. R. Miller, and S. J. Simpson. From disorder to order in marching locusts. *Science*, 312:1402–1406, 2006.

[7] P-L. Buono and R. Eftimie. Analysis of Hopf/Hopf bifurcations in nonlocal hyperbolic models for self-organised aggregations. *Math. Models Methods Appl. Sci.*, 24(2):327–357, 2014.

[8] A. Cavagna, A. Cimarelli, I. Giardina, G. Parisi, R. Santagati, F. Stefanini, and R. Tavarone. From empirical data to inter-individual interactions: unveiling the rules of collective animal behavior. *Math. Models Methods Appl. Sci.*, 20:1491–1510, 2010.

[9] Y.-L. Chuang, M.R. D'Orsogna, D. Marthaler, A.L. Bertozzi, and L.S. Chayes. State transitions and the continuum limit for a 2D interacting, self-propelled particle system. *Physica D*, 232:33–47, 2007.

[10] I. D. Couzin, J. Krause, R. James, G.D. Ruxton, and N. R. Franks. Collective memory and spatial sorting in animal groups. *J. Theor. Biol.*, 218:1–11, 2002.

[11] R. Eftimie. *Modeling group formation and activity patterns in self-organizing communities of organisms*. PhD thesis, University of Alberta, 2008.

[12] R. Eftimie. Hyperbolic and kinetic models for self-organised biological aggregations and movement: a brief review. *J. Math. Biol.*, 65(1):35–75, 2012.

[13] R. Eftimie, G. de Vries, and M. A. Lewis. Complex spatial group patterns result from different animal communication mechanisms. *Proc. Natl. Acad. Sci.*, 104(17):6974–6979, 2007.

[14] R. Eftimie, G. de Vries, M. A. Lewis, and F. Lutscher. Modeling group formation and activity patterns in self-organizing collectives of individuals. *Bull. Math. Biol.*, 69(5):1537–1566, 2007.

[15] R. Eftimie, G. de Vries, and M.A. Lewis. Weakly nonlinear analysis of a hyperbolic model for animal group formation. *J. Math. Biol.*, 59:37–74, 2009.

[16] R. Fetecau and R. Eftimie. An investigation of a nonlocal hyperbolic model for self-organization of biological groups. *J. Math. Biol.*, 61(4):545–579, 2010.

[17] S.E. Folias. Nonlinear analysis of breathing pulses in a synaptically coupled neural network. *SIAM J. Applied Dynamical Systems*, 10(2):744–787, 2011.

[18] M. Golubitsky and I. Stewart. *The Symmetry Perspective: from equilibrium to chaos in phase space and physical space*. Birkhäuser, Basel, 2002.

[19] M. Golubitsky, I. Stewart, and D.G. Schaeffer. *Singularities and Groups in Bifurcation Theory. Volume 2*. Springer-Verlag New York Inc., 1988.

[20] D. Grünbaum. Schooling as a strategy for taxis in a noisy environment. *Evol. Ecol.*, 12:503–522, 1998.

[21] S. Gueron, S. A. Levin, and D. I. Rubenstein. The dynamics of herds: from individuals to aggregations. *J. Theor. Biol.*, 182:85–98, 1996.

[22] S. Guo. Equivariant Hopf bifurcation for functional differential equations of mixed type. *Appl. Math. Letters*, 24:724–730, 2011.

[23] D. Helbing and P. Molnar. Social force model for pedestrian dynamics. *Phys. Rev. E*, 51(5):4282–4286, 1995.

[24] C. K. Hemelrijk and H. Kunz. Density distribution and size sorting in fish schools: an individual-based model. *Behav. Ecol.*, 16(1):178–187, 2004.

[25] A. Hill and I. Stewart. Hopf-steady-state mode interactions with **0(2)** symmetry. *Dynamics and Stability of Systems*, 6(2):149–170, 1991.

[26] T. Hillen. Existence theory for correlated random walks on bounded domains. *Canad. Appl. Math. Quart*, 18(1):1–40, 2010.

[27] H.J. Hupkes and S.M. Verduyn Lunel. Center manifold theory for functional differential equations of mixed type. *J. Dyn. Differential Equations*, 19:497–560, 2007.

[28] A. Huth and C. Wissel. The simulation of fish schools in comparison with experimental data. *Ecol. Model*, 75/76:135–145, 1994.

[29] O. Igoshin, A. Mogilner, R. Welch, D. Kaiser, and G. Oster. Pattern formation and traveling waves in myxobacteria: Theory and modeling. *Proc. Natl. Acad. Sci. USA*, 98:14913–14918, 2001.

[30] I. Kmit and L. Recke. Fredholm alternative for periodic-Dirichlet problems for linear hyperbolic systems. *J. Math. Anal. Appl.*, 335(1):355–370, 2007.

[31] M. Kovacic. On matrix-free pseudo-arclength continuation methods applied to a nonlocal pde in 1+1d with pseudo-spectral time-stepping. Master's thesis, University of Ontario Institute of Technology, 2013.

[32] R. Li and B. Bowerman. Symmetry breaking in biology. *Cold Spring Harbor Perspectives in Biology*, 2:a003475, 2010.

[33] A.J. Lotka. *Elements of physical biology*. Williams & Wilkins Company, 1925.

[34] R. Lukeman, Y.-X. Li, and L. Edelstein-Keshet. Inferring individual rules from collective behavior. *Proc. Natl. Acad. Sci USA*, 107(28):12576–12580, 2010.

[35] M.Lichtner, M. Radziunas, and L. Recke. Well-posedness, smooth dependence and centre manifold reduction for a semilinear hyperbolic system from laser dynamics. *Math. Meth. Appl. Sci.*, 30:931–960, 2007.

[36] A. Mogilner and L. Edelstein-Keshet. A non-local model for a swarm. *J. Math. Biol.*, 38:534–570, 1999.

[37] J. Murray. *Asymptotic analysis*. Springer, Heidelberg, 1984.

[38] J.K. Parrish and L. Edelstein-Keshet. Complexity, pattern, and evolutionary trade-offs in animal aggregations. *Science*, 284(2):99–101, 1999.

[39] J.K. Parrish, S.V. Viscido, and D. Grünbaum. Self-organised fish schools: an examination of emergent properties. *Biol. Bull.*, 202:296–305, 2002.

[40] H. Pomeroy and F. Heppner. Structure of turning in airborne rock dove (*Columba Livia*) flocks. *The Auk*, 109:256–267, 1992.

[41] W. K. Potts. The chorus-line hypothesis of manoeuvre coordination in avian flocks. *Nature*, 309:344–345, 1984.

[42] D. V. Radakov. *Schooling in the ecology of fish*. John Willey & Sons Inc, New York, 1973.

[43] S. Springer. Some observations of the behavior of schools of fishes in the gulf of mexico and adjacent waters. *Ecology*, 38:166–171, 1966.

[44] C. M. Topaz and A. L. Bertozzi. Swarming patterns in a two-dimensional kinematic model for biological groups. *SIAM J. Appl. Math*, 65(1):152–174, 2004.

[45] C. M. Topaz, A. L. Bertozzi, and M. A. Lewis. A nonlocal continuum model for biological aggregation. *Bull. Math. Biol.*, 68:1601–1623, 2006.

[46] C. M. Topaz, M.R. D'Orsogna, L. Edelstein-Keshet, and A.J. Bernoff. Locust dynamics: behavioral phase change and swarming. *PLoS, Comput. Biol.*, 8:e1002642, 2012.

[47] K. Warburton and J. Lazarus. Tendency-distance models of social cohesion in animal groups. *J. Theor. Biol.*, 150:473–488, 1991.

[48] J.L. Yorzinski and G.L. Patricelli. Birds adjust acoustic directionality to beam their anti predatory calls to predators and conspecifics. *Proc. R. Soc. B*, 277(1683):923–932, 2010.